Analysis of vulnerability to reentry in acute myocardial ischemia using a realistic human heart model

Edison F. Carpio[1,2], Juan F. Gomez[3], José F. Rodríguez-Matas[4], Beatriz Trenor[1], José M. Ferrero[1*]

[1] Centre for Research and Innovation in Bioengineering (Ci2B), Universitat Politècnica de València, Valencia, Spain.
[2] University of Cuenca, Cuenca, Ecuador.
[3] Valencian International University, Valencia, Spain.
[4] LabS, Department of Chemistry, Materials and Chemical Engineering "Giulio Natta", Politecnico di Milano, Milano, Italy

*** Corresponding author**
E-mail address: cferrero@ci2b.upv.es (JMF)
Postal address: Centre for Research and Innovation in Bioengineering (Ci2B), Universitat Politècnica de València, Camino a Vera s/n, Valencia, Spain

* **Keywords:** Acute myocardial ischemia, computational modeling, His-Purkinje system, ventricular arrhythmias, vulnerability to reentry.

Abstract

Electrophysiological alterations of the myocardium caused by acute ischemia constitute a pro-arrhythmic substrate for the generation of potentially lethal arrhythmias. Experimental evidence has shown that the main components of acute ischemia that induce these electrophysiological alterations are hyperkalemia, hypoxia (or anoxia in complete artery occlusion), and acidosis. However, the influence of each ischemic component on the likelihood of reentry is not completely established. Moreover, the role of the His-Purkinje system (HPS) in the initiation and maintenance of arrhythmias is not completely understood. In the present work, we investigate how the three components of ischemia affect the vulnerable window (VW) for reentry using computational simulations. In addition, we analyze the role of the HPS on arrhythmogenesis. A 3D biventricular/torso human model that includes a realistic geometry of the central and border ischemic zones with one of the most electrophysiologically detailed model of ischemia to date, as well as a realistic cardiac conduction system, were used to assess the VW for reentry. Four scenarios of ischemic severity corresponding to different minutes after coronary artery occlusion were simulated. Our results suggest that ischemic severity plays an important role in the generation of reentries. Indeed, this is the first 3D simulation study to show that ventricular arrhythmias could be generated under moderate ischemic conditions, but not in mild and severe ischemia. Moreover, our results show that anoxia is the ischemic component with the most significant effect on the width of the VW. Thus, a change in the level of anoxia from moderate to severe leads to a greater increment in the VW (40 ms), in comparison with the increment of 20 ms and 35 ms produced by the individual change in the level of hyperkalemia and acidosis, respectively. Finally, the HPS was a necessary element for the generation of approximately 17% of reentries obtained. The retrograde conduction from the myocardium to HPS in the ischemic region, conduction blocks in discrete sections of the HPS, and the degree of ischemia affecting Purkinje cells, are suggested as mechanisms that favor the generation of ventricular arrhythmias.

1 Introduction

Electrophysiological heterogeneities in the myocardium caused by acute ischemia can lead to potentially lethal arrhythmias, such as ventricular tachycardia (VT) and ventricular fibrillation (VF) [1]. Indeed, within the first 10 to 15 minutes after a coronary artery occlusion and the subsequent lack of blood flow, the patient frequently suffers sudden cardiac death due to the appearance of arrhythmias [2].

Experimental evidence has shown that two discrete phases of ventricular arrhythmias occur within the first 30 minutes of myocardial ischemia [3,4]. Phase 1A takes place between 2 and 10 min of ischemia approximately [4], with reentry as the predominant mechanism of origin . VT is the most common arrhythmia in this stage [5,6]. Phase 1B occurs within 18 – 30 min after artery occlusion [4], although the main mechanisms for triggering arrhythmias are not precisely defined [6,7]. A great number of VF events and larger mortality has been reported during this stage [8,9]. However, the overall incidence of arrhythmias is higher during phase 1A [8].

Electrophysiological changes at the cellular and intercellular levels occur during acute myocardial ischemia and predispose the heart to the occurrence of arrhythmias [10]. It is well known that the three main ischemic components that induce electrophysiological alterations in the affected tissue are hyperkalemia, hypoxia (or anoxia, in the case of complete coronary artery occlusion), and acidosis [11,12]. Within the acute phase of ischemia, hyperkalemia (i.e., an increase of extracellular potassium concentration, $[K^+]_o$) generally reduces conduction velocity (CV) and cell excitability, and induces post-repolarization refractoriness [10,13]. Anoxia (i.e., absence of oxygen supply) shortens the action potential duration (APD) [14,15], while acidosis (i.e., a reduction of pH) affects the behavior of certain ionic currents [16,17]. All these alterations occur in a heterogeneous way through the myocardium, providing the pro-arrhythmic substrate for the occurrence of reentrant arrhythmias [13].

The influence of the main ischemic components in arrhythmogenesis has been investigated in the past. However, due to the complex process of acute myocardial ischemia, the relative contributions of each component are still not completely established. Experimental and simulation studies have analyzed the combined effect of hyperkalemia, anoxia, and acidosis [11,18–20], as well as the effect of one component at a time during the generation of arrhythmias [11,21,22]. Although some researchers have suggested the existence of a predominant ischemic component favoring the likelihood of arrhythmias [18,19,23], there are no works that have assessed and compared the individual influence of the three components simultaneously using a realistic 3D anatomical model during ischemia. A 2D simulation study by Trenor et al. [19] evaluated the individual effect of these components. However, a realistic ischemic region and HPS were not included in their work.

The role of the HPS as a possible element that favors the onset and maintenance of ventricular arrhythmias also needs further investigation. Experimental recordings of the HPS electrical activity have provided some evidence supporting the implication of the HPS in VF. For instance, experiments in canines showed retrograde and anterograde propagation between the myocardium and the HPS during VF [24]. In another study, endocardial cryoablation in pig hearts modified the activation pattern of VF [25]. Finally, a faster extinction of VF was observed in dogs after chemical ablation of Purkinje fibers [26]. Despite all these evidences, results in animals do not always translate to human due to differences between species. In addition, the acquisition techniques of these studies may be not sufficient to measure the HPS electrical activity without recording the surrounding activity. Therefore, the role of the HPS in the onset and maintenance of ventricular arrhythmias is controversial, and complex to assess experimentally in humans.

Computational simulations are a useful and complementary tool to analyze ischemia-induced arrhythmias and the role of the HPS. Several simulation studies have assessed the likelihood of arrhythmias within the first minutes of acute ischemia by the quantification of the vulnerable window (VW) [19,20,22,27]. The VW is defined as time interval during which ectopic stimuli can elicit a reentry. However, there are few ischemic simulation studies that include a detailed HPS [28,29], and also a realistic ischemic region in a human ventricular model [30].

In this work, we investigate the effects of hyperkalemia, anoxia, and acidosis on the VW to reentry during different ischemic scenarios involving different severities of ischemia. In addition, we analyze the role of the HPS and its mechanisms of action in the generation and propagation of reentrant activity. These studies were carried out using a 3D biventricular human model that includes a realistic geometry of the ischemic central and border zones, as well as the cardiac conduction system.

2 Methods

2.1 Anatomical model

In the present study, we used a 3D anatomical model of the ventricles including a realistic geometry of the ischemic region previously developed by our group (Fig 1) [31]. The biventricular model was built from manual segmentation of a DE-MRI stack using Seg3D software (Scientific Computing and Imaging Institute, University of Utah, USA) [32]. A surface model of the ventricles was generated from the segmented images and meshed using MeshGems-Hexa (Distene S.A.S., Bruyeres-le-Chatel, France), obtaining a volume mesh formed of 4 million nodes (vertices) and 3.71 million hexahedral elements, with an average edge length of 0.4 mm. Transmural heterogeneity of the ventricular myocardium was assigned in the model by defining endocardial, mid-myocardial, and epicardial zones, which were adjusted to 17%, 41%, and 42% of the ventricular wall thickness, respectively [33–35]. Myocardial anisotropy was implemented by defining fiber orientation based on the method by Streeter et al. [36].

The biventricular model was based on cardiac DE-MRI images from a patient that revealed ischemic myocardial regions in the LV. Using the American Heart Association (AHA) nomenclature, these regions were located in the medial and basal segments of both inferolateral and inferoseptal walls (segments 3, 5, 9, and 11), and all segments of the inferior wall (apical, mid-cavity, and basal) (segments 4, 10, and 15), mainly associated with an occlusion of the right coronary artery (RCA) [37]. To overcome the limitations of other previous models that consider geometrically simple ischemic and border zones [22,27,38], we used realistic regions corresponding to chronic infarction. Although it is well known that infarcted areas do not totally match the area of acute ischemia, simulations on an anatomical model based on experimental data will always be closer to reality. Indeed, after myocardial ischemia has developed, the damaged tissue evolves and changes significantly both in structure, size [39] and function, as does the border zone [40]. The process of infarct healing is indeed complex and determined by many factors [41]. For the sake of simplicity, in our model the 3D geometries of the ischemic central zone (ICZ) and the border zone (BZ) (Fig 1A and Fig 1B) were obtained by applying the standard deviation (SD) method [42] during the segmentation of the DE-MRI stack. Briefly, the myocardium was divided into healthy and ischemic regions based on the gray color intensity of each pixel. Similarly, the ischemic region was categorized as ICZ or BZ. ICZ was assigned for pixel intensities higher than mean value + 3×SD of healthy tissue; BZ for pixel intensities between mean + 2×SD and mean + 3×SD values; and healthy tissue (or normal zone (NZ)) for pixel intensities below mean + 2×SD. The different regions were mapped into the volume mesh of the ventricles and each hexahedral element was labeled as ICZ, BZ or NZ (Fig 1A and Fig 1B). For further details regarding the biventricular model construction, see [31].

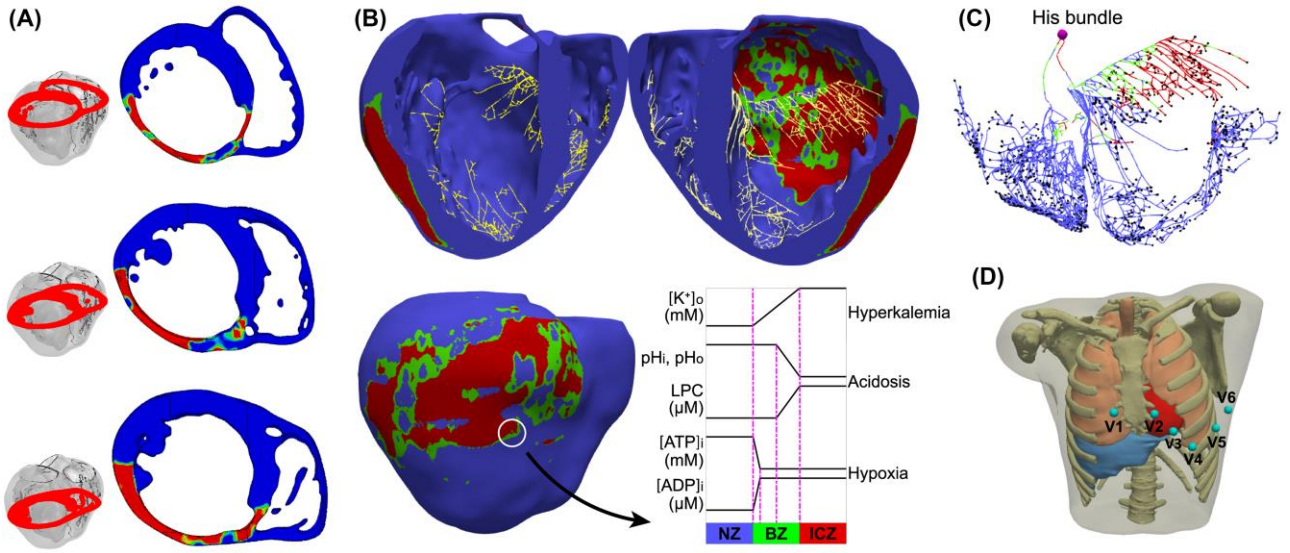

Fig 1. Anatomical model. (A) Short axis cross-sectional views of the biventricular model at three different levels showing a representation of the ischemic region (ICZ in red and BZ in green) and the normal zone (NZ in blue) reconstructed from the DE-MRI images. (B) Endocardial (upper) and epicardial (lower) views of the biventricular model in acute ischemia. The ischemic central zone (ICZ) (red), the border zone (BZ) (green), the normal zone (NZ) (blue), the His-Purkinje system (HPS) (yellow), and the spatial variations of $[K^+]_o$, $[ATP]_i$, $[ADP]_i$, pH_i, pH_o, and LPC across the different zones are shown. (C) HPS with its elements labeled as ICZ (red), BZ (green), and NZ (blue). Purkinje-Muscle junctions are represented as small brown spheres. (D) Torso model, including the biventricular mesh (red) and the precordial leads location.

The HPS network used in our simulations was the same network developed in our previous work [43]. It was built based on a stochastic growth method [44] using linear elements. The right ventricle (RV) and left ventricle (LV) sections of the network comprised two and three main branches with several subdivisions, respectively. A total of 1391 Purkinje-Muscle junctions (PMJs) were distributed across the myocardium, which, upon simulation, yielded a typical ECG wave morphology in the precordial leads. Furthermore, we adjusted the conductivity of the PMJs so as to allow retrograde and anterograde electrical propagation as it has been experimentally observed [45]. Finally, each HPS element was labeled as NZ, ICZ or BZ depending on its location (Fig 1C).

To compute the ECG in the precordial leads, we fitted the biventricular model into a torso mesh previously developed [46], using a linear transformation. The adjusted torso mesh comprised 1.26 million nodes and 7.35 million tetrahedral elements, with a spatial resolution of 0.55mm (Fig 1D). Furthermore, tissue conductivities of lungs, liver, bones, blood pools, great vessels, and skeletal muscle were included in the torso model. For further detailed information, see [31].

2.2 Action potential model in acute ischemia

As the basal model for our simulations, we used a modified version of the O'Hara action potential (AP) model [47] and we introduced it into our 3D biventricular model as in our previous work [43]. To include changes related to acute ischemia (hyperkalemia, anoxia, and acidosis) in the model, we modified several currents and incorporated others, as in [48,49].

To introduce the effects of the ischemic factors (intracellular ATP ($[ATP]_i$) and ADP ($[ADP]_i$), intracellular and extracellular pH (pH_i and pH_o, respectively) and intracellular LPC ($[LPC]_i$)), we followed the ischemic model previously published and validated by our group [48]. Briefly, we

introduced the following changes in the AP model. First, we incorporated the ATP-sensitive K^+ current ($I_{K(ATP)}$) proposed by Ferrero et al. [15], which was adapted to human ventricular myocytes by modifying the maximum conductance and the sensitivity to $[ATP]_i$ and $[ADP]_i$ using data from Babenko et al. [50]. Second, we introduced different scaling factors in the formulations of the Na^+/K^+, sarcolemmal Ca^{2+} and SERCA pumps that depend on $[ATP]_i$ and $[ADP]_i$ as in the model proposed by Cortassa et al. [51]. To introduce the effects of acidosis in the model, we modified the inactivation (f_{ss}) and activation (d_{ss}) gates of the L-type Ca^{2+} current (I_{CaL}) and multiplied the maximum conductance by a scaling factor to mimic the experimental results observed by Saegusa et al. [17]. Furthermore, we multiplied the fast and late Na^+ currents (I_{Na} and I_{NaL}, respectively) and the Na^+/K^+ pump by different scaling factors that depend on extracellular and intracellular pH (pH_o and pH_i, respectively), and lysophosphatidylcholine (LPC). The effects of pH_o and pH_i were obtained from [52–55], while those due to LPC were obtained from [56–58]. Finally, the effect of hyperkalemia was introduced by simply increasing the $[K^+]_o$.

The values of $[K^+]_o$, $[ATP]_i$, $[ADP]_i$, pH_i, pH_o, and LPC used in the AP model were chosen in correspondence to four different severities of acute ischemia in the ICZ: mild (≈ 2.5 minutes after occlusion), moderate (≈ 5 minutes after occlusion), moderate-severe (≈ 7.5 minutes after occlusion), and severe (≈ 10 minutes after occlusion) (see Fig 2). The values for healthy and severe conditions were taken within a range of experimental data [14,56,59–62]. Parameter values for mild, moderate, and moderate-severe conditions were calculated using linear interpolation, except for $[K^+]_o$. For the latter, we used a Boltzmann curve which approximately mimics the behavior of the $[K^+]_o$ during the first 10 – 15 minutes of ischemia in accordance with several experimental studies [61–64] (Fig 2).

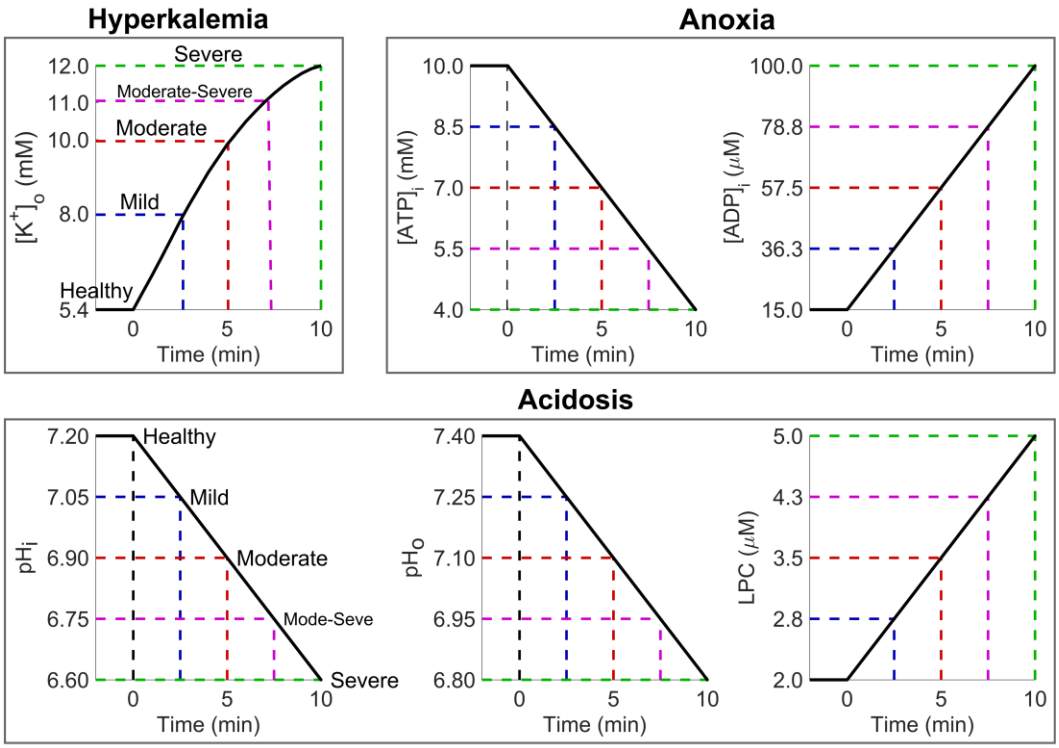

Fig 2. Time course of ischemia-related parameters during the first 10 minutes of acute ischemia. Parameter values before arterial occlusion (t = 0) correspond to healthy conditions. Parameter values for 2.5, 5.0, 7.5, and 10.0 minutes of ischemia correspond to a mild (blue traces), moderate (red traces), moderate-severe (magenta traces), and severe (green traces) ischemic condition, respectively.

Within the BZ, the morphology and extension of which was derived from the DE-MRI images as explained above, we implemented a nonlinear gradient of each ischemic-related parameter from its physiological value in the NZ to its ischemic value in the ICZ, as shown in experimental studies [65,66]. The gradient was defined by means of a steady state diffusion problem (Laplace equation)

in which all nodes within the ICZ were given a value of one and all nodes within the NZ were given a value of zero. Then, the spatial distribution of the different ischemic-related parameters was mapped into the model based on the value of the scalar field within the BZ. The transition within the BZ occurred along its entire width for $[K^+]_o$, along the 50% of the BZ (next to the ICZ) for pH_i, pH_o, and LPC, and along the proximal 10% of the BZ (next to the NZ) for $[ATP]_i$ and $[ADP]_i$ (see Fig 1B, bottom panel). Figure 3 shows the distribution of $[K^+]_o$, $[ADP]_i$, and pH_o for the moderate case.

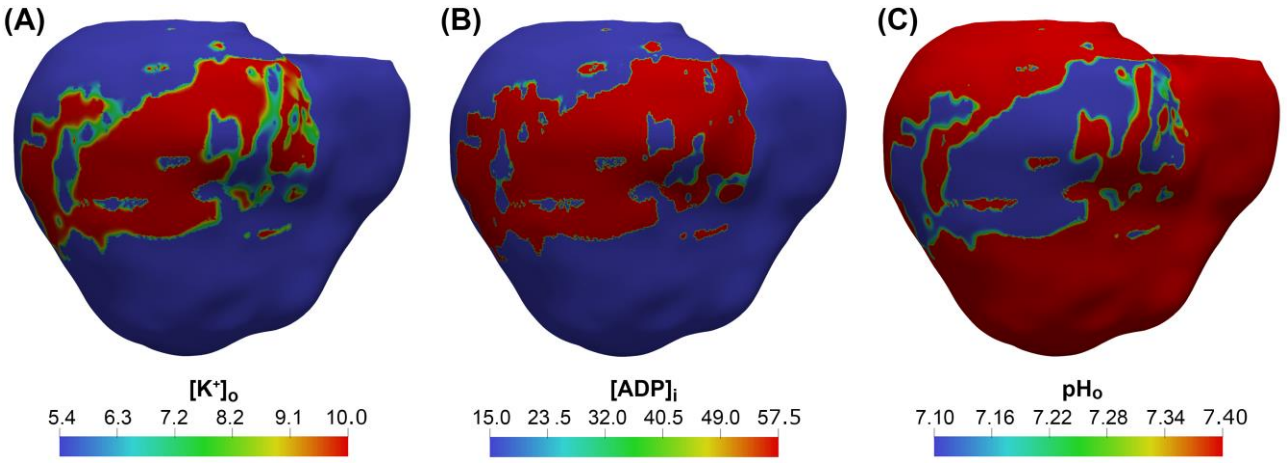

Fig 3. Spatial distribution of ischemic-related parameters for the moderate case. (A) $[K^+]_o$ distribution, (B) $[ADP]_i$ distribution, and (C) pH_o distribution. See text for details.

Ischemic simulations including the HPS were performed using the AP model of Purkinje cells developed by Stewart et al. [67], which is commonly accepted. The effects of hyperkalemia on Purkinje cells were introduced in the model by simply increasing the $[K^+]_o$ as in the nearest cardiomyocyte. The effects of anoxia and acidosis were not introduced due the lack of experimental information.

2.3 Stimulation protocol

In the present study, we analyzed the role of each ischemic component (hyperkalemia, anoxia, and acidosis), as well as the role of the HPS, in the generation of reentries. For this purpose, our 3D human ventricular model with and without the HPS was used to simulate the bioelectric behavior of the ventricles under different acute ischemic conditions. In the presence of the HPS, sinus rhythm was simulated by applying an electrical stimulus (S1) in the hypothetical location where the bundle of His begins. Conversely, when the HPS was removed from the model, a stimulus was applied at each location of a PMJ at the same instant in which the PMJ was activated in the simulation with the HPS. Seven consecutive beats with a cycle length of 600 ms were simulated in both cases. After the fifth beat of the series, a premature stimulus (S2) was applied in a region of the epicardial BZ in the mid posterior LV wall. This stimulus mimics the earliest epicardial activity experimentally observed in the myocardium adjacent to the border zone after a premature beat occurred in acute ischemia [68]. The time interval between the fifth S1 and S2 (coupling interval or CI) was varied with a resolution of 5 ms to determine the duration of the VW for reentry. The range of CIs that produced at least two reentrant cycles in the biventricular model was defined as the VW. Approximately a total of 100 simulations were conducted combining the 3D anatomical model with and without HPS, different ischemic severity scenarios and several CIs. Simulations were executed in a node with 64 processors, taking 2 hours to simulate 100 ms of electrical activity in the ventricles and HPS. Thus, a complete simulation of seven heart beats (≈ 4800 ms) took around 4 days to be completed.

2.4 Numerical methods

Simulations were run using ELVIRA software [69]. The electrical propagation throughout the ventricles was computed by solving the reaction-diffusion monodomain equation

$$\nabla \cdot (\boldsymbol{D} \nabla V_m) = C_m \frac{\partial V_m}{\partial t} + I_{ion} + I_{stim} \quad (1)$$

where $\boldsymbol{D}$ is the equivalent conductivity tensor, V_m is transmembrane potential, C_m is membrane capacitance, I_{ion} is transmembrane ionic current and I_{stim} is the transmembrane stimulation current. This system of differential equations that results from equation 1 plus the ordinary differential equations related to gating and dynamic changes in ionic concentrations [69] was solved using the finite element method (FEM).

To obtain a realistic CV in the biventricular model, we performed a set of test simulations on a 3D slab model of 20 mm x 20 mm x 8 mm as in our previous study [43]. The longitudinal (σ_L) and transversal (σ_T) conductivities were fit to 0.5 S/m and 0.1 S/m, respectively. This calibration yielded a CV of 0.61 m/s along the fiber direction and of 0.29 m/s perpendicular to the fiber direction, in accordance with experimental measurements in human ventricles [70]. For the HPS, the CV was adjusted to 2.5 m/s approximately [71,72].

The ECG and the body surface potential maps (BSPM) were obtained using an approximation of the bidomain approach. Specifically, the transmembrane potentials computed in the nodes of the hexahedral biventricular mesh were interpolated to the nodes of the tetrahedral torso mesh that corresponded to the ventricular myocardium. Then, the extracellular potentials (φ_e) in the ventricles were calculated by solving the passive term of the bidomain approach

$$\nabla \cdot ([\boldsymbol{D_i} + \boldsymbol{D_e}] \nabla \varphi_e) = -\nabla \cdot (\boldsymbol{D_i} \nabla V_m) \quad (2)$$

where $\boldsymbol{D}_i$ and $\boldsymbol{D}_e$ are the volume-averaged conductivity tensors of the intra and extracellular domains, respectively [73,74]. Subsequently, applying Dirichlet boundary conditions at the ventricles-torso interface and Neumann-type conditions at the torso surface, the extracellular potentials were computed in the whole domain of the 3D torso model (Ω_T) by using the FEM method to solve the following Laplace equation:

$$\nabla \cdot (\boldsymbol{D_T} \cdot \nabla V_T) = 0 \quad \text{in} \quad \Omega_T \quad (3)$$

where V_T represents extracellular potentials within the domain of the torso model (except for the ventricles) and $\boldsymbol{D}_T$ is the heterogeneous conductivity tensor of the torso model defining its conductive properties [31]. We assigned isotropic conductivities to each tissue (see [43] for details). Finally, the ECG in each precordial lead was computed as the extracellular potential at the electrode location referred to the Wilson Central Terminal, as done in the clinical practice. The total activation time (TAT) of the ventricular mesh was estimated as the time interval between the first and last depolarized node in the mesh above a threshold of −10mV.

3 Results

3.1 Changes in electrical activation and ECG under different severities of acute ischemia

Figure 4A shows ventricular activation maps under healthy conditions and under three different severities of acute ischemia. In non-pathological conditions, endocardial activation of the LV

started 18 ms after the His stimulation, and 9 ms later the RV activation began. This results are similar to those obtained by Durrer et al. in human hearts [71]. The TAT of the ventricles was approximately 100 ms, comparable to [71,75]. The last activated part in the LV was the anterolateral region, while the latest areas depolarized in the RV were the outflow tract and posterobasal regions.

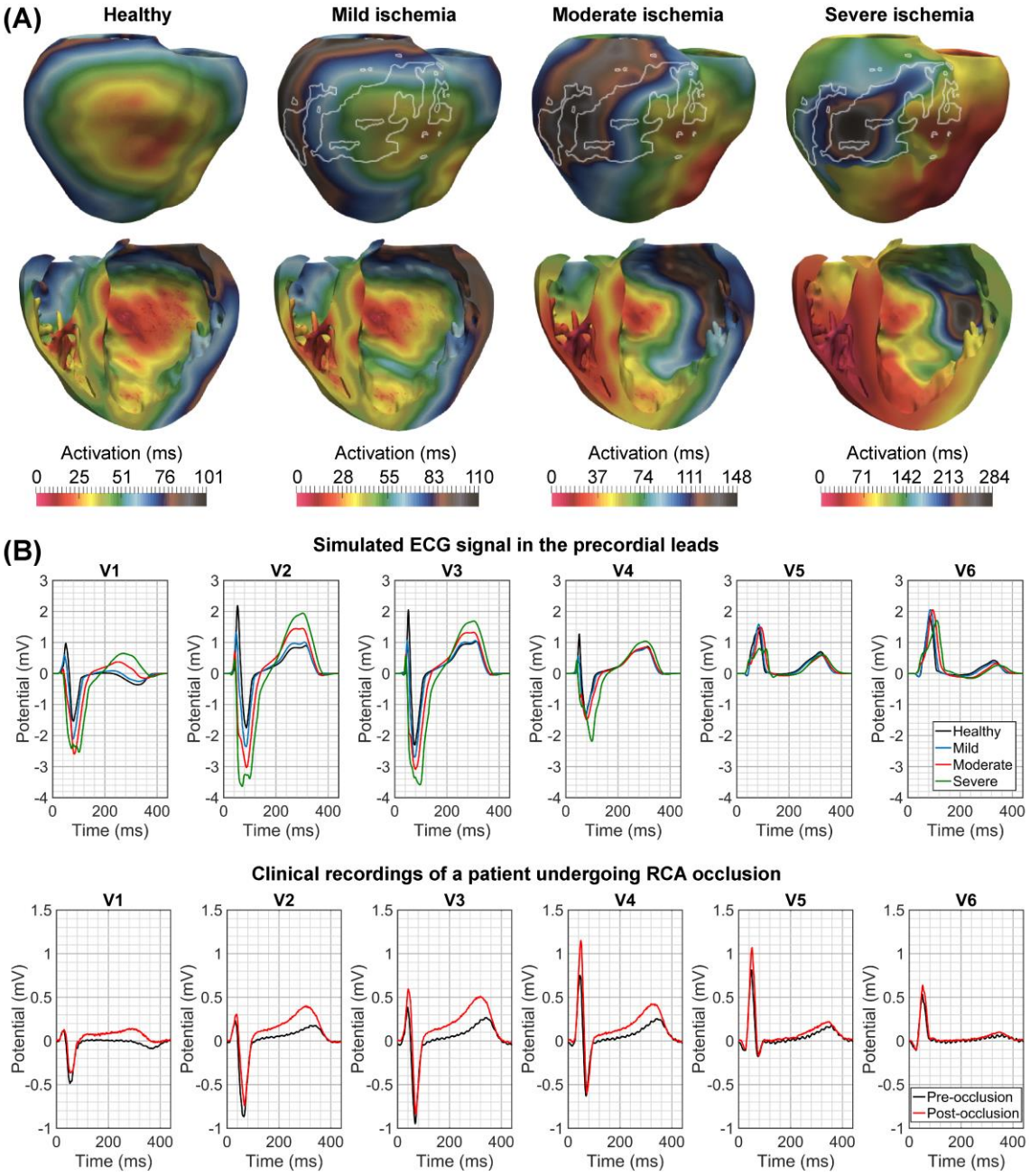

Fig 4. Simulated myocardial activation maps and ECG signals under different ischemic severities. (A) Posterior view (top row) and anterior cross-sectional view (bottom row) of the biventricular model showing the activation on the epicardium (upper) and endocardium and mid-myocardium (lower), respectively. White curves represent the ischemic central zone. (B) Comparison between simulated precordial lead signals (top row) and clinical recordings of a patient before and 3 minutes after an RCA occlusion (bottom row). Patient data were taken from the STAFF III database of the Physionet repository [76].

Under ischemic conditions, the electrical conduction in the sections of the HPS located in the ischemic region was slower. This reduction in the propagation velocity led to a delay in the onset of ventricular activation. Accordingly, when mild ischemia was simulated, the LV and RV activation started at 26 ms and 30 ms, respectively. During moderate ischemia conditions, the electrical

impulse from the His bundle arrived first to the RV endocardium at 34 ms, while the LV activation started 7 ms after the onset of RV activation. In severe ischemia, the first activation in the RV and LV occurred at 40 ms and 69 ms, respectively. Furthermore, a wavefront from the RV reached the LV endocardium in the apical septal region at 74 ms, which depolarized the apex and the endocardial lateral wall through myocardial propagation and retrograde conduction through the HPS. In this last case, an incomplete left bundle branch block (LBBB) was observed.

Similarly, a reduced conduction velocity in the ischemic region led to a progressive increase in the TAT and a change in the latest activated area. In mild ischemic conditions, the activation of the whole myocardium took 110 ms. The last activated areas in the RV were the same regions than in healthy conditions. However, the latest area depolarized in the LV was shifted slightly to the lateral region. During moderate ischemic conditions, the TAT was increased to 148 ms and the latest activated region in the LV was the posterolateral wall next to the ICZ. Under severe ischemic simulations, a marked increase in the TAT to 248 ms was obtained. In addition, the ICZ was the latest activated region, although in healthy conditions this region was one of the first parts of the LV epicardial wall to be activated.

Figure 4B shows a comparison between the computed ECG in the precordial leads for simulations in a healthy heart and under three different severities of acute ischemia (top panel), and clinical recordings of a patient before and 3 minutes after an RCA occlusion (bottom panel). Data were taken from the Physionet repository (https://physionet.org/), STAFF III database, patient 8 [76,77]. In non-pathological conditions, the duration of the QRS complex (QRSd) was approximately 90 ms, in accordance with human data [78,79]. Under ischemic conditions, the QRSd was increased to 98, 121, and 133 ms for mild, moderate, and severe ischemia, respectively. This last value supports the diagnosis of an incomplete LBBB, caused by a reduced conduction velocity in the main branches of the HPS probably due to the severe level of ischemia.

Several changes in the T-wave morphology of the precordial leads were observed during ischemic simulations. Our results show an increment in the T-wave amplitude, especially in leads V2 and V3, similarly to the clinical record of the example patient after RCA occlusion (red trace), as recorded as well in clinical practice [80]. In addition, a transition of the T-wave in lead V1 from negative in healthy conditions to a biphasic behavior during moderate ischemia (≈ 5 min after the onset of ischemia) was found, which agrees with the clinical recording 3 minutes after RCA occlusion (red trace). This finding is considered very specific of ischemia [80,81]. For severe ischemic conditions, an inverted T-wave was obtained in lead V1, in accordance with experimental data [80].

Finally, an elevation of the ST segment in leads V1–V3 was measured at the J point (end of the QRS complex) for a moderate ischemic condition (8, 110, and 100 µV, respectively). This alteration was also observed in the clinical ECG, although in a different degree (71, 81, and 70 µV). Conversely, the simulated ECG under severe ischemia displayed a marked ST depression of –426, –573, and –457 µV in leads V1–V3 compared to non-pathological tissue. This depression represents the combined effect of acute ischemia and LBBB, which is in accordance with the second criterion of Sgarbossa (ST segment depression ≥ 1 mm in V1, V2, and/or V3) for the diagnosis of a patient with these two pathologies [82,83].

3.2 Effect of acute ischemia in the action potential

Figure 5 shows the alterations in APD and resting membrane potential (RMP) during mild, moderate, and severe acute ischemia. As shown in Fig 5A, simulations under ischemic conditions produced APD shortening, a reported effect in patients with this pathology [84]. In healthy conditions, the APD values ranged 232 – 347ms, depending on the location within the ventricles.

The longest APDs were found in PMJ sites on the endocardial wall, whereas the shortest APDs were found in sites close to the latest electrically activated area on the epicardium wall, which is in accordance with experimental observations [29,85,86].

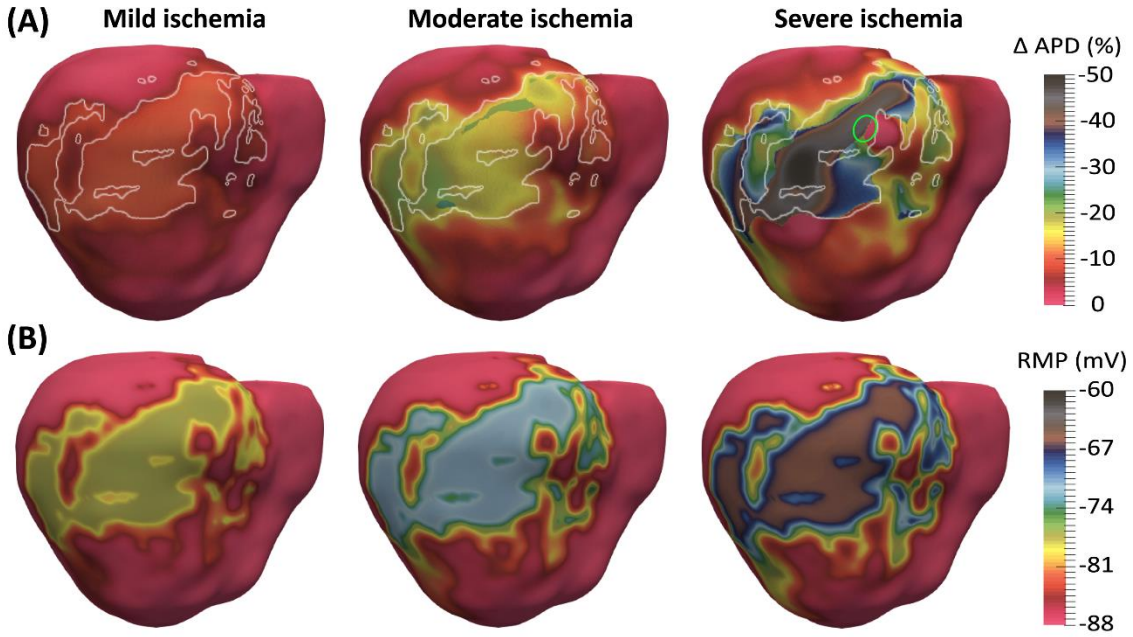

Fig 5. Electrophysiological changes in the action potential under acute ischemia. Simulated maps of action potential duration (APD) variation (A) and resting membrane potential (RMP) (B) under mild, moderate and severe ischemia conditions. The white curves represent the ischemic central zone (ICZ), while the green circle shows the epicardial region within the ICZ where spatial heterogeneity was greater.

Under pathological conditions, the longest APDs remained localized at the functional PMJs, which is in accordance with [29], whereas the shortest APDs were found in the ischemic region. Under mild, moderate, and severe ischemia, APD was reduced by a maximum of 18%, 27%, and 49% of the normal values, which agrees with [84]. Furthermore, the degree of APD shortening varied spatially throughout the ischemic tissue, as reported in other studies [87]. This spatial heterogeneity was greater during severe ischemia. Coexisting areas were found inside the ICZ with and without APD reduction ($\Delta APD = 45\%$ and $\Delta APD = 0\%$, respectively) (Fig 5A, green circle). To investigate the differences in APDs in this region, we analyzed the propagation patterns. Our results show that a wavefront entering the ICZ from its right side was able to stimulate the proximal ICZ, maintaining the peak potential and avoiding APD reduction in the region. However, the central section of the ICZ was stimulated by several wavefronts of reduced amplitude that led to APD shortening.

Similarly, our results (Fig 5B) show a less negative RMP under acute ischemia conditions, as in previous experimental and simulation studies [19,88,89]. In non-pathological tissue, the RMP was approximately –88mV, while in the ICZ RMP was –73mV, –68mV, and –63mV for mild, moderate, and severe ischemia, respectively. In the BZ, resting potentials values varied between the healthy and ischemic values.

3.3 Role of acute ischemia in the generation of reentries

In order to assess the effect of the degree of ischemia in the generation of reentry, the VW during each ischemic condition was calculated by applying a premature stimulus (S2) in an area of the border zone in the epicardial wall (point P1 in Fig 6), as explained in the Methods section. S2 was delivered at different time intervals (coupling intervals) after the fifth sinus (S1) beat. Figure 6A shows the VW obtained during four different ischemic severities: mild, moderate, moderate-severe, and severe. Our results predict a VW of approximately 5 ms in moderate ischemic conditions,

corresponding to a CI between 335 and 340 ms. A change in the ischemic severity to a moderate-severe condition yielded the maximum width of the VW (45 ms), with a range of CIs between 345 and 390 ms. Conversely, no reentries were found from mild or severe conditions. In summary, our results suggest that the ischemic severity plays an important role in the generation of reentries. A unimodal behavior of the VW during the first 10 minutes of ischemia was observed. In other words, a premature stimulus applied only in a moderate (≈ 5 minutes after occlusion) or moderate-severe level (≈ 7.5 minutes after occlusion) of acute ischemia could generate a reentry.

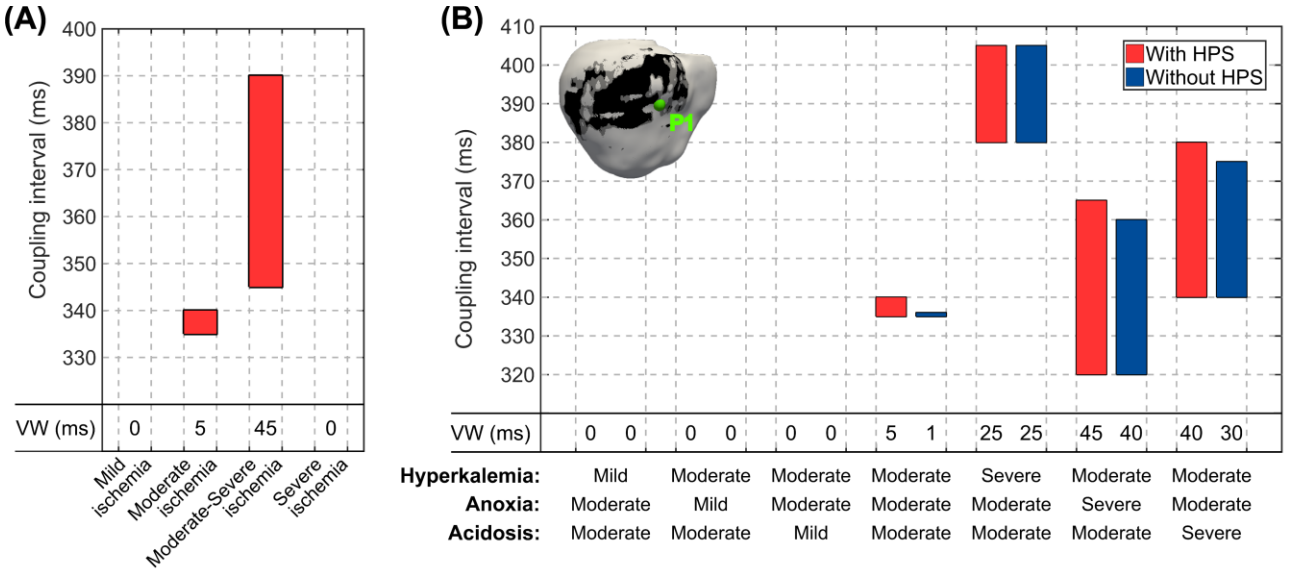

Fig 6. Vulnerable window (VW) to reentry. (A) VW under four different ischemic severities: mild, moderate, moderate-severe, and severe. These conditions correspond to 2.5, 5.0, 7.5, and 10.0 minutes of ischemia, respectively. (B) VW under seven different scenarios of acute ischemia. The severity of each ischemic component (hyperkalemia, anoxia, and acidosis) in each scenario is shown at the bottom. Red and blue bars represent the results of simulations with and without the HPS, respectively. Stimulation point (P1) of the premature stimulus is show in light green inside the inset.

To evaluate the effects of each ischemic component (hyperkalemia, anoxia, and acidosis) on the generation of reentries, we quantified the VW during seven different scenarios of acute ischemia in the biventricular model with and without the HPS (Fig 6B). Each scenario corresponded to different severities of each of the three components of ischemia (e.g. mild hyperkalemia + moderate acidosis + moderate anoxia). Computational simulations in the model that included the HPS (red bars) showed a VW approximately of 5 ms under a moderate ischemic level in all components, with CIs originating reentries between 335 and 340 ms. An individual change of hyperkalemia, anoxia or acidosis from moderate to severe led to an increment to 25 ms in the VW with CIs between 380 and 405 ms, 45 ms with CIs between 320 and 365 ms, and 40 ms with CIs between 340 and 380 ms, respectively. Conversely, no reentry (VW = 0 ms) was found during the individual reduction of each ischemic parameter to mild.

On the other hand, computational simulations in the model without the HPS (Fig 6B, blue bars) yielded reentries only for a CI = 335 ms under moderate ischemic conditions for all components of ischemia. An individual change of hyperkalemia, anoxia or acidosis level from moderate to severe led to an increase in the VW to 25 ms with CIs between 380 and 405 ms, 40 ms with CIs between 320 and 360 ms, and 35 ms with CIs between 340 and 375 ms, respectively. Finally, any change of any ischemic component from moderate to mild did not generate reentries (VW = 0 ms).

The influence of the HPS in the width of the VW was analyzed in the different scenarios. Results without HPS, but maintaining the normal sinus activation by stimulating the PMJ locations (as described in the Methods section), showed slight reductions in the VW width (blue bars in Fig 6B)

with respect to simulations including the HPS (red bars). Under moderate ischemic conditions, the VW was reduced to less than 5 ms. An increment in the hyperkalemia level from moderate to severe did not produce changes in the VW between simulations with and without retrograde conduction (VW = 25 ms). On the other hand, when anoxia or acidosis were individually increased to the severe level, the VW was reduced in 5 ms in simulations without the HPS. Furthermore, the suppression of the retrograde conduction through the HPS affected the VW only for the highest CI values (blue blocks). In summary, our results show that anoxia has the most significant effect on the width of the VW and that the HPS is a fundamental element in the generation of reentry for higher CI values of the VW. Furthermore, the HPS provides propagation pathways favoring the maintenance of reentry.

The most common reentrant pattern observed during our acute ischemia simulations was a figure-of-eight reentry, which is in accordance with many experimental observations [10,68,90]. Also, the position, size and pattern of the reentrant circuit changed from beat to beat. Figure 7 shows the propagation patterns of a macroreentry obtained in our biventricular model including the HPS. Simulated ischemic conditions were moderate hyperkalemia and acidosis, and severe anoxia. Reentrant activity started with a premature stimulus (S2) in the right BZ occurring 320 ms after the fifth sinus beat (S1). In the first reentrant cycle, a unidirectional block within the ICZ (straight line, second row) gave rise to two circus movements around it, which were completed at 310 ms after S2 (third row). In the HPS, wavefronts were propagated by means of both retrograde and anterograde conduction.

In the second reentrant cycle, the reentrant pattern also showed two circus movements. The lower circus movement was established around a zone of conduction block located in the lower part of the ischemic region. The diameter of the block region was approximately 1.5 cm. The circus movement ended at 630 ms after S2 (fourth and fifth rows). The upper circus movement was established around the ICZ. This wavefront was combined with a fragmented wavefront coming from the lower circus movement, and this gave rise to the third cycle. In the HPS, a temporary conduction block was observed in two sections located on the septal wall (fourth row in Fig 7A).

During the third cycle of the reentry, two circus movements around the ICZ and another propagation circuit throughout the ICZ were established. The wavefront from the ICZ was combined with the upper wavefront. Later, both the lower and upper wavefronts were also combined to retrogradely cross the ICZ. During this same cycle, a wavefront was transmurally propagated to give rise to reentrant activity in the endocardium (black circle, fifth row). In the HPS, a new wavefront was generated in one of the RV PMJs due to current flow from the myocardium to the HPS. This event was produced during the repolarization of the RV septum when the HPS section located in the septum was able to allow electrical conduction (black circle, last row) (see Video 1).

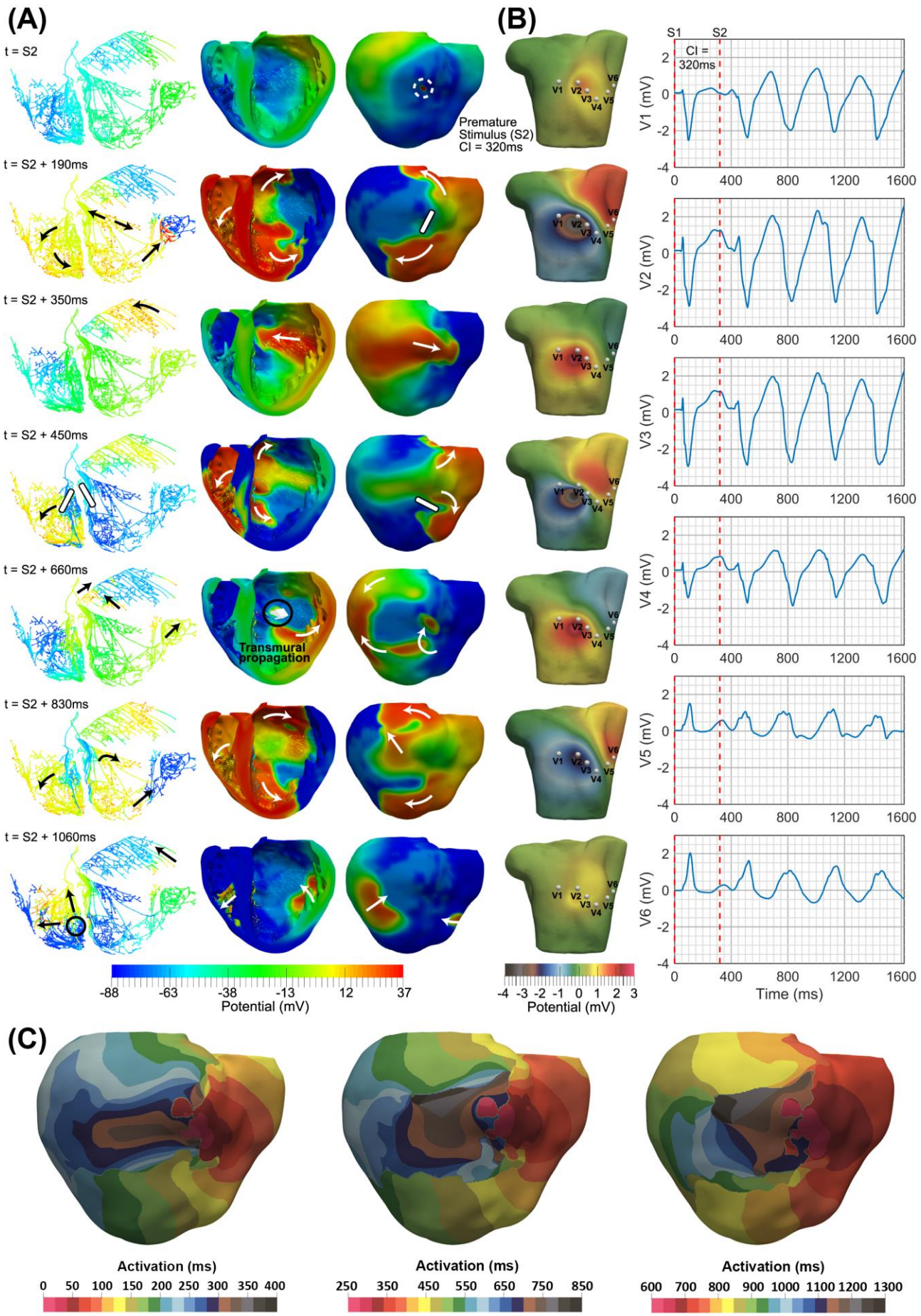
(A)
t = S2
t = S2 + 190ms
t = S2 + 350ms
t = S2 + 450ms
t = S2 + 660ms
t = S2 + 830ms
t = S2 + 1060ms
Transmural propagation
-88 -63 -38 -13 12 37
Potential (mV)
(B)
Premature Stimulus (S2) CI = 320ms
V1 V2 V3 V4 V5 V6
-4 -3 -2 -1 0 1 2 3
Potential (mV)
S1 S2
CI = 320ms
V1 (mV)
V2 (mV)
V3 (mV)
V4 (mV)
V5 (mV)
V6 (mV)
0 400 800 1200 1600
Time (ms)
(C)
Activation (ms)
0 50 100 150 200 250 300 350 400
Activation (ms)
250 350 450 550 650 750 850
Activation (ms)
600 700 800 900 1000 1100 1200 1300

Fig 7. Reentrant pattern of a macro-reentry using the biventricular/torso model. (A) Ventricular potential maps that show the generation of a figure-of-eight reentry. The simulated ischemic conditions were moderate hyperkalemia and acidosis, and severe anoxia. Arrows indicate the propagation direction of the wavefront, while the straight lines indicate unidirectional conduction block. The black circle in the last row shows the location where a new wavefront was generated due to current flow from the myocardium to HPS. (B) Body surface potential maps and ECG recorded at precordial leads during the reentry. (C) Epicardial activation maps showing activation times during the first (left), second (middle) and third (right) reentry cycles.

Figure 7B displays the body surface potential maps and the ECG obtained during this particular reentry. As shown in the figure, positive and negative potential areas were registered on the torso during each reentrant cycle. A rotary clockwise pattern seems to occur in different planes. In that sense, when a reentrant cycle begins, a region of positive potential appears near the location of leads V2 and V3. Then, this region moves towards the left shoulder and from that site to the lower part of the back. Finally, the zone of positive potential returns to its initial location, giving rise to a new cycle. A clear example of this movement can be seen in the ECG computed in the precordial leads (Fig 7B, right). The ECG shows the typical pattern of a ventricular tachycardia with a mean cycle length of around 320 ms (which corresponds to approximately 188 beats per minute).

Figure 7C shows epicardial activation maps corresponding to the first (left), second (middle) and third (right) reentry cycles obtained in the simulation. The activation times, color-coded in the figure, correspond to the three cycles of reentry shown in Fig 7A and in Video 1.

3.4 Role of the His-Purkinje system in the generation of reentry

Figure 8 illustrates the role of the HPS in the generation of reentry during moderate ischemia elicited with a premature stimulus (S2) 340 ms after the onset of the last sinus beat. In the model including the HPS, a sustained reentry of at least 3 reentrant cycles was obtained (Figs 8A, and 8C blue trace). Conversely, no reentry was generated under the same ischemic conditions when the HPS was removed from the model (Figs 8B, and 8C red trace). In this last case, a bidirectional conduction block was observed at the right border of the ICZ.

When the S2 stimulus was applied (first row), a conduction block in the ICZ produced two reentrant circuits in both scenarios (second row). This fragmented wavefront proceeded retrogradely into the ICZ and entered the NZ, sustaining the reentry during the simulation with the HPS (Fig 8A, third row). Conversely, the fragmented wavefront entered the ICZ but was blocked in the still refractory NZ in the simulation without HPS (Fig 8A, third row). Our results reveal a slow conduction velocity in the ischemic region for both scenarios. However, areas with high PMJs density within the ischemic region had a further slight reduction in conduction velocity due to current flowing from the myocardium to the HPS during the wavefront propagation through the myocardium (see Video 2). This slower conduction velocity in the simulations with the HPS allowed the NZ to recover once the wavefront had crossed the ICZ.

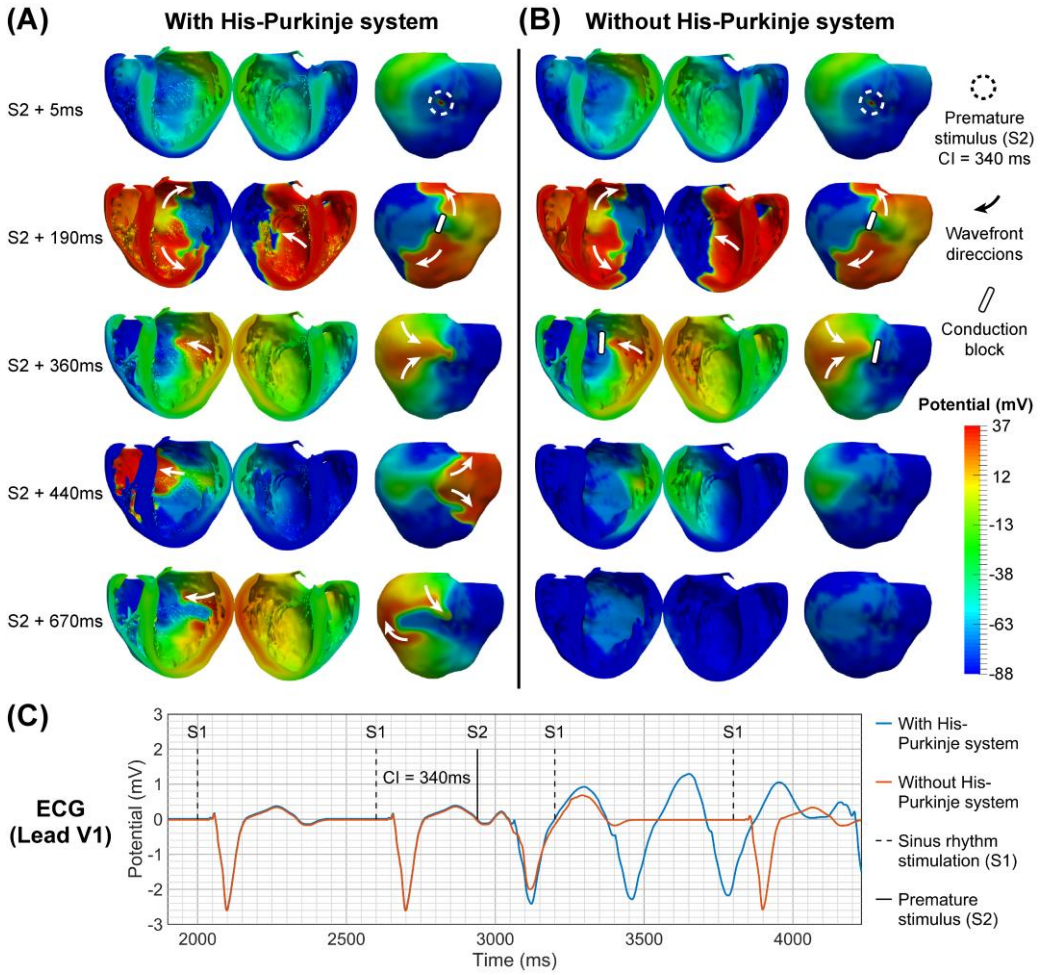

Fig 8. Role of the His-Purkinje system on reentry generation. (A) Macro-reentry obtained with the model that includes the HPS. (B) No reentry in the ischemic simulation using the model without HPS. (C) ECG simulated in lead V1 for both cases. Simulations were performed under moderate ischemia.

4 Discussion

In this study, a set of acute ischemic simulations were performed in a 3D biventricular/torso model with a realistic ischemic region and cardiac conduction system. We analyzed the influence of the three main components of ischemia (hyperkalemia, anoxia, and acidosis) and the role of the HPS in reentry generation. Our simulations were performed using a modified version of the O'Hara et al. [47] action potential model in which we included the main ionic changes related to acute ischemia. The simulations results obtained with the model are in accordance with previous experimental and simulation studies and shed light into the mechanisms responsible for reentrant activity during acute ischemia.

The major findings of this study are the following. First, the severity of ischemia plays an essential role in determining the likelihood of reentrant arrhythmic activity. The worst scenario for arrhythmia development is moderate ischemia. Second, the single ischemic component with the most significant effect on the VW for reentry was anoxia. Third, the retrograde conduction from the myocardium to the HPS in the ischemic region plays a decisive role in reentry generation for higher CI values within the VW. Fourth, the hyperkalemia level in Purkinje cells affects the generation of reentries. And fifth, the maintenance of the sinus excitation overlapped with the reentrant activity does not significantly alter the wavefront propagation in the arrhythmic myocardium.

4.1 Role of ischemic severity in the generation of reentries

During the first 10 – 15 minutes of acute myocardial ischemia, metabolic changes in the injured tissue produce a series of electrical alterations in the affected cells, such as APD shortening, CV reduction and RMP increment to less negative values [19,66,70,84]. These ischemia-induced alterations are not homogeneous within the ischemic region, but appear in the form of gradients between the ICZ and the BZ [65,87]. In our study, simulation results for different severities (or minutes) of acute ischemia were consistent with the experimental and simulation data mentioned above. A combined effect of hyperkalemia, anoxia, and acidosis due to ischemia led to a dispersion of refractoriness and CV in the ischemic myocardium, setting the pro-arrhythmic substrate for reentries generation [65,91].

Previous experimental observations during acute myocardial ischemia reported that arrhythmias occur in two distinct phases: before 10 minutes, and between 20 and 40 minutes after coronary artery occlusion [6,8,91]. In our study, we only analyzed the appearance of arrhythmic activity during the first 10 minutes of ischemia. According to our results, reentries were triggered between the first 5 to 7.5 minutes of ischemia (moderate to moderate-severe ischemic conditions), corresponding with said first phase of arrhythmias. These results are also in agreement with the studies performed by Smith et al. [8] and Kaplinsky et al. [92], which reported that reentries occur 2 to 10 minutes after the occlusion, with the peak of arrhythmic events at 5 to 6 minutes approximately. Similarly, Morena et al. [11] reported a high occurrence of arrhythmias between 3 and 8 minutes after the occlusion of the left anterior descending artery (LAD) in pigs. Finally, in the study by Coronel et al. VF was induced with one ventricular premature beat after 5 minutes of ischemia, but not after 10 minutes during LAD occlusion in perfused porcine hearts [21]. For this last experiment, an $[K^+]_o$ value between 8.0 and 13.5 mM was a necessary condition for the induction of VF.

In our simulations, reentries were generated for values of $[K^+]_o$ of 10 and 11 mM, which is in accordance with [21]. Also, in the study by Hirche et al. [63], $[K^+]_o$ levels between 10.7 ± 1.9 and 14 ± 2.9 mM were measured during the first phase of ventricular arrhythmias in pigs with acute coronary artery occlusion. Conversely, Tobar et al. [22] in their simulation study reported that reentries were not generated for values of $[K^+]_o$ greater than 9 mM. A possible explanation between the different results obtained in the present study and the one by Tobar et al. [22] lies on the most recent action potential model used in our simulations and the most realistic form of modeling the effects of acute ischemia in the AP ventricular model. In addition, the simulation study by Martinez-Navarro et al. [27] reported reentries for $[K^+]_o$ = 9.5 mM using the O'Hara model. This value is close to the levels of $[K^+]_o$ that induced reentries in our study. However, in the work by Martinez-Navarro et al. [27] a realistic ischemic region and a detailed HPS were not included, as in the present research study.

Finally, our study showed that in terms of the role of ischemia severity on reentry generation there are not many qualitative differences between the results obtained with our anatomical model, which considers a realistic ischemic region, and other studies using models with geometrically simpler ischemic regions (commonly a circular shape) [19,22]. Indeed, a higher incidence of reentries was observed in both cases under moderate ischemic conditions. However, irregularities in the realistic ischemic region can be important to define the reentrant pattern, as observed in our simulations.

4.2 Separate role of the ischemic components in the generation of reentries

Cells affected by acute ischemia experience hyperkalemia, anoxia, and acidosis due to the lack of blood flow [63,93]. However, the influence of each ischemic component on arrhythmogenesis is difficult to analyze experimentally. For this purpose, computational models have become an

important tool in understanding the mechanisms responsible for reentry. For instance, Ferrero et al. [23] used computational simulations to analyze the mechanisms involved in figure-of-eight reentry in a ring-shaped 1-dimensional strand of cardiac cells. The results of this study suggested that the most pro-arrhythmic ischemic component would be anoxia. Subsequently, the same group studied the role of each ischemic component in the establishment of figure-of-eight reentry in a 2D model [20]. They reported that a sustained reentry can be generated under conditions of strong hyperkalemia alone ($[K^+]_o$ > 11.9 mmol/L), and that severe anoxia tends to reduce myocardial vulnerability to reentry. Similar results were reported in the study by Trenor et al. [19]. In the latter, the authors observed that a lower hyperkalemia ($[K^+]_o \leq 11$ mmol/L) level did not lead to reentry generation regardless of the presence of anoxia or acidosis. In addition, a similar role of acidosis and anoxia in the widening of the VW was reported in this study. Both computational analyses were performed using the Luo-Rudy AP model [94]. On the other hand, a more recent study by Tobar et al. [22] investigated the effects of hyperkalemia on the VW for reentry using the ten Tusscher AP model [95] in a 3D biventricular mesh. Their results showed that $[K^+]_o$ had a significant effect on the size of the VW. However, effects of anoxia and acidosis were not analyzed.

In our study, a modified version of the O'Hara AP model was used to evaluate the individual effects of hyperkalemia, anoxia, and acidosis in the width of VW for reentry. From a moderate ischemic severity in the three ischemic components, an individual change of a single ischemic component to mild or severe conditions was applied, resulting in a total of seven scenarios of ischemic severity analyzed (see Fig 6B). Our model showed that all components of ischemia affect the VW, although in a different degree and via different mechanisms. Indeed, our simulation results suggest that anoxia has the most significant effect on the width of the VW, i.e., anoxia could be the most pro-arrhythmic individual component of ischemia in accordance with Ferrero et al. [23]. However, this effect was only slightly major (a difference of 5 ms) compared to a change in acidosis alone, which brings our results closer to the observations reported by Trenor et al. [19], who observed a similar effect of anoxia and acidosis on the VW. The recent study by Lawson et al. [96] demonstrated that the wavelength (calculated as the product of APD times CV) is the most critical factor in reentry initiation, with anoxia being the primary determinant of this factor, while acidosis had a minor effect. However, the authors mentioned that their results may underestimate the role of the lack of oxygen due to simplifications adopted by the reduced ten Tusscher ionic model used in their study. Experimentally, the relative contribution of each ischemic component to the genesis of ventricular arrhythmias is not established. That said, Wilde, in his review study about the role of ATP-sensitive K^+ channel current in ischemic arrhythmias, reported that the activation of the $I_{K(ATP)}$ current (activated by anoxia) in the early phase of acute ischemia potentially contributes to the development of ventricular arrhythmias [97]. Moreover, the study by Said et al. [98] suggests that the presence of acidosis in perfused rat hearts may affect intracellular calcium management, causing the initiation of arrhythmias.

On the other hand, our study also shows that hyperkalemia was the ischemic component with less effect in the VW. Despite this, a minimum value of $[K^+]_o$ of 10 mM was necessary to trigger a reentry even in the presence of moderate anoxia and acidosis. This result suggests that hyperkalemia level could play an important role in reentry generation, in agreement with the simulation study by Tobar et al. [22] and with the experimental study by Morena et al. [11]. In the latter, the regional combination of anoxia with acidic perfusion did not generate early arrhythmia in porcine hearts. However, when anoxia was combined with a $[K^+]_o$ around 10 mM, VT was observed after 10 minutes and VF after 20 minutes. A similar result was reported in the study performed in dogs by Senges et al. [18].

Finally, our model shows that an individual and combined change of the three ischemic components could produce opposite effects in the VW width. Indeed, an increment solely of hyperkalemia, anoxia, or acidosis to severe conditions led to a widening of the VW, while the

simultaneous increment of all components reduced the VW to 0 ms (i.e., no reentries were observed). This result shows the importance of the concomitant effects of the ischemic components on arrhythmogenesis, in accordance with other studies [18,21]. In the work by Senges et al. [18] in canine hearts, the regional combination of anoxia plus lactic acidosis, without hyperkalemia, failed to trigger reentrant arrhythmias, which were indeed observed when regional hyperkalemia was included. Similar results were reported in the study by Coronel et al. [21], which analyzed the effects on the arrhythmogenesis of both hyperkalemia and ischemia (i.e., all ischemic components). The results of their experiments showed that a reentrant arrhythmia could be generated in a tissue with $[K^+]_o$ between 8 and 13.5 mM, but only in hypoxic and acidotic conditions.

4.3 Role of the His-Purkinje system in the generation of reentries

The role of the HPS in the generation and maintenance of ventricular arrhythmias is controversial. Experimental studies, such as Cha et al. [99] have reported that in the absence of the HPS, VF in dogs could continue but at a slower rate. Other study by Livia et al. [100] observed that the elimination of Purkinje fibers with irreversible electroporation reduced the threshold/vulnerability toward VF induction during an experiment with 8 canine hearts. Conversely, Janse et al. [101] reported that after the destruction of the subendocardium including the HPS, ectopic beats in the myocardium were triggered by ischemia, but none of these beats degenerated into VF.

In our study, simulation results showed a slight reduction of the VW when the HPS was removed from the biventricular model, in accordance with experimental observations reported by Livia et al. [100]. The inclusion of the HPS in the anatomical model played a double role in the generation of reentry. First, the HPS played an irrelevant role in the generation of reentrant activity in approximately 83% of the simulations where reentries were generated and sustained. This means that reentries were triggered without the need for HPS in 83% of the simulations. However, when the HPS was included in the model, reentrant circuits which included the HPS in their pathways were observed in all simulations, as in [28,102]. These circuits allowed an earlier activation of distant regions to the ischemic zone through retrograde and anterograde fast conduction, which suggests that the HPS could help to maintain a reentry as in the simulation study by Deo et al. [28]. In the latter work, authors reported that propagation pathways throughout the HPS prolong the arrhythmic activity and that the HPS plays an additional role in maintaining the later stages of reentry, although the CIs range for reentry inducibility in simulations with and without the HPS were similar. Second, in our simulations the inclusion of the HPS in the biventricular model was a necessary condition in the generation of reentries for higher CI values within the VW, opposite to the simulation results obtained by Deo et al. [28]. Indeed, our simulations revealed that the HPS further reduces conduction velocity in the ischemic region with high density of PMJs. This additional reduction allowed the NZ to recover once the wavefront had crossed the ICZ, generating a reentry.

Although our results indicate that the HPS plays an important role in the generation of reentries, they also suggest that this role depends on the degree of hyperkalemia that affects Purkinje cells. To confirm this observation, simulations under moderate ischemia were repeated in the biventricular model including the HPS, but without the effects of hyperkalemia in Purkinje cells (results not shown), i.e. no changes were made to the Purkinje AP model in ischemic conditions [29]. This change was applied in order to mimic the resistance of Purkinje to ischemia observed in several experimental studies [99,103]. Under this consideration, no reentries were found for moderate ischemic conditions (VW = 0 ms). These results were different to the ones obtained in simulations that included the effects of hyperkalemia in the Purkinje cell (VW $\approx$ 5 ms). An explanation for the different behaviors lies on the slow CV and conduction blocks in discrete sections of the HPS due to hyperkalemia. These effects led to a delay in ventricular activation that allowed the recovery of

excitability in areas of the NZ stimulated by the premature stimulus (S2). Thus, a wavefront that propagates throughout the ICZ is able to re-stimulate the repolarized tissue. Our results are in agreement with experimental observations previously reported [104,105]. These studies proved that slow conduction through discrete regions of Purkinje fibers subject to high $[K^+]_o$ may result in reentrant arrhythmias. Similar results were obtained in the study by Senges et al. [18] performed in the canine ventricular conduction system. In the latter study, researchers also observed that during regional anoxia or lactic acidosis, no arrhythmias were generated, while regional increases of $[K^+]_o$ may be the predominant ischemic component to generation of reentrant arrhythmias.

Whenever reentry was induced, a typical figure-of-eight reentrant pattern was obtained in all our simulations with the biventricular model, as reported in canine and porcine hearts [10,68,90]. Changes in location, revolution time and size were observed in a beat-to-beat basis during each reentry. However, a changing reentrant pattern (e.g. a circus and double circus pattern) was obtained with the model that includes the HPS, similar to those observed by Janse et al. [10,68]. All our reentries showed a VT pattern which did not evolve in VF, in accordance with other studies in animals [8,9,106]. In these studies, evolution from VT into VF was rare during the first phase of ischemic arrhythmias (phase 1A of arrhythmias).

Experimental evidence on the effects of heart rate on the occurrence of ventricular arrhythmias is scarce. Observations in dog hearts by Chadda et al. [107] have suggested that the sinus rhythm could be related with the initiation of ventricular arrhythmias. In this study, the authors observed that after coronary occlusion the incidence of VT and VF occurs mainly at slow and rapid heart rates. On the other hand, our simulation results showed that a sustained sinus rhythm at 100 beats/min (BCL = 600 ms) does not induce the generation or abolition of reentries. This result is supported by Sung et al. [108], who reported that tachycardia triggered by potential delayed afterdepolarizations, could be initiated by accelerating the sinus rate, but only in 3 of 21 patients with clinical evidence of recurrent sustained VT. Another study performed in 262 subjects during 6 hours of infarction observed primary VF in 20 patients [109]. Within this group, 7 patients developed tachycardia, 10 had a sinus rate between 60 – 100 beats/min and 2 bradycardia immediately prior to VF. In summary, our results together with the experimental evidence, suggest that the effects of heart rate on reentry generation could vary among patients.

5 Study Limitations

An AP model of Purkinje cells that includes the effects of the main ischemic components has yet to be developed due to the lack of experimental information. Several studies in animals have reported that the HPS is more resistant to the effects of ischemia than cardiomyocytes, with many Purkinje fibers surviving after infarcts [103,110,111]. However, during the initial phase of acute ischemia it is not certain whether, or to what extent, the subendocardial Purkinje fibers change their electrophysiological properties. In this study, effects of anoxia and acidosis in Purkinje cells were not simulated while hyperkalemia was introduced by increasing the $[K^+]_o$ as in the nearest cardiomyocyte. This $[K^+]_o$ increment has been reported as the potential predominant factor of the ischemic components that facilitates the onset of reentrant arrhythmias in Purkinje cells [18]. Although our results have been compared with experimental studies and clinical observations, a most realistic model of the effects of acute ischemia in the HPS could alter our results. Thus, the main findings should be carefully validated both in a set of computational models of different patients (with different HPS configurations) and in clinical studies.

To quantify the VW for reentry, a premature stimulus was applied in a region of the BZ. However, the location of the stimulation region in the BZ has been shown to affect the VW [27]. For this reason, a future study should investigate whether the effect of the three main ischemic

components in the width the VW could be influenced by the location of the premature stimulus or by the location of the ischemic region in the heart.

It is well known that the size, shape and position of the ischemic region plays an important role on the genesis and maintenance of reentry. However, MRI images are very difficult to obtain during the acute ischemia stage in human hearts *in-vivo*. Consequently, changes in the extension of the ischemic central and border regions over time [39-41] are complex to model realistically. In our study, simulations were performed in a 3D anatomical model with a static ischemic region size, due to the lack of clinical evidences.

6 Conclusion

In this study, we used a biventricular human model that includes a realistic ischemic region and a cardiac conduction system to investigate the influence of each ischemic component in the VW for reentry. Our anatomical model, together with the more detailed ventricular AP model used to simulate acute myocardial ischemia, allowed us to obtain reentrant patterns corresponding to experimental ventricular tachycardia. The main findings of this study showed that ischemic severity plays an important role in the generation of reentries. Specifically, reentries can be only generated under intermediate ischemic conditions. Furthermore, our results also showed that anoxia is the ischemic component with the most significant effect on the width of the VW. In the analysis of the role of the HPS during acute myocardial ischemia, our results showed that its inclusion in the anatomical model was decisive for reentry generation for higher CI values of the VW.

Author contribution

JR, BT and JF contributed to the conception and design of the study, with the participation of EC. Computational simulations were performed by EC. The analysis/interpretation of the results was performed by EC, JG, BT, and JF. All authors contributed to draft the manuscript and all authors revised and approved the submitted version.

Funding

This work was supported by the Secretaría de Educación Superior, Ciencia, Tecnología e Innovación (SENESCYT) of Ecuador CIBAE-023-2014, by Grant PID2019-104356RB-C41 funded by MCIN/AEI/ 10.13039/501100011033, by the European Union's Horizon 2020 research and innovation programme under grant agreement No 101016496, by Dirección General de Política Científica de la Generalitat Valenciana (PROMETEO 2020/043), and by the "Programa Salvador de Madariaga 2018" of the Spanish Ministry of Science, Innovation and Universities (Grant Reference PRX18/00489).

References

[1] J.T. Vermeulen, H.L. Tan, H. Rademaker, C.A. Schumacher, P. Loh, T. Opthof, R. Coronel, M.J. Janse, Electrophysiologic and extracellular ionic changes during acute ischemia in failing and normal rabbit myocardium, J. Mol. Cell. Cardiol. 28 (1996) 123–131. https://doi.org/10.1006/jmcc.1996.0012.

[2] D.P. Zipes, H.J.J. Wellens, Sudden Cardiac Death, Circulation. 98 (1998) 2334–2351. https://doi.org/10.1161/01.CIR.98.21.2334.

[3] M.J. Janse, A.L. Wit, Electrophysiological mechanisms of ventricular arrhythmias resulting from myocardial ischemia and infarction, Physiol. Rev. 69 (1989) 1049–1169. https://doi.org/10.1152/physrev.1989.69.4.1049.

[4] M.J. Janse, R. Coronel, F.J.G. Wilms-Schopman, J.R. De Groot, Mechanical effects on

arrhythmogenesis: From pipette to patient, Prog. Biophys. Mol. Biol. 82 (2003) 187–195. https://doi.org/10.1016/S0079-6107(03)00015-4.
[5] S.M. Pogwizd, P.B. Corr, Reentrant and nonreentrant mechanisms contribute to arrhythmogenesis during early myocardial ischemia: results using three-dimensional mapping, Circ. Res. 61 (1987) 352–371. https://doi.org/10.1161/01.RES.61.3.352.
[6] W.E. Cascio, Myocardial Ischemia: What Factors Determine Arrhythmogenesis?, J. Cardiovasc. Electrophysiol. 12 (2001) 726–729. https://doi.org/10.1046/j.1540-8167.2001.00726.x.
[7] A.B. Chicos, A.H. Kadish, Arrhythmias in Coronary Artery Disease, in: Electrophysiol. Disord. Hear., 2nd ed., Saunders, 2012: pp. 825–834.
[8] W.T. Smith, W.F. Fleet, T.A. Johnson, C.L. Engle, W.E. Cascio, The Ib Phase of Ventricular Arrhythmias in Ischemic In Situ Porcine Heart Is Related to Changes in Cell-to-Cell Electrical Coupling, Circulation. 92 (1995) 3051–3060. https://doi.org/10.1161/01.CIR.92.10.3051.
[9] F.M. McDonald, H. Knopf, S. Hartono, W. Polwin, A. Bischoff, H. Hirche, K. Addicks, Acute myocardial ischaemia in the anaesthetised pig: local catecholamine release and its relation to ventricular fibrillation, Basic Res. Cardiol. 81 (1986) 636–645. https://doi.org/10.1007/BF02005187.
[10] M.J. Janse, A.G. Kléber, Electrophysiological changes and ventricular arrhythmias in the early phase of regional myocardial ischemia, Circ. Res. 49 (1981) 1069–1081. https://doi.org/10.1161/01.RES.49.5.1069.
[11] H. Moréna, M.J. Janse, J.W. Fiolet, W.J. Krieger, H. Crijns, D. Durrer, Comparison of the effects of regional ischemia, hypoxia, hyperkalemia, and acidosis on intracellular and extracellular potentials and metabolism in the isolated porcine heart, Circ. Res. 46 (1980) 634–646. https://doi.org/10.1161/01.RES.46.5.634.
[12] I. Kodama, A. Wilde, M.J. Janse, D. Durrer, K. Yamada, Combined effects of hypoxia, hyperkalemia and acidosis on membrane action potential and excitability of guinea-pig ventricular muscle, J. Mol. Cell. Cardiol. 16 (1984) 247–259. https://doi.org/10.1016/S0022-2828(84)80591-X.
[13] E. Carmeliet, Cardiac ionic currents and acute ischemia: From channels to arrhythmias, Physiol. Rev. 79 (1999) 917–1017. https://doi.org/10.1152/physrev.1999.79.3.917.
[14] J.N. Weiss, N. Venkatesh, S.T. Lamp, ATP-sensitive K^+ channels and cellular K^+ loss in hypoxic and ischaemic mammalian ventricle., J. Physiol. 447 (1992) 649–673. https://doi.org/10.1113/jphysiol.1992.sp019022.
[15] J.M. Ferrero, J. Sáiz, J.M. Ferrero, N. V. Thakor, Simulation of Action Potentials From Metabolically Impaired Cardiac Myocytes, Circ. Res. 79 (1996) 208–221. https://doi.org/10.1161/01.RES.79.2.208.
[16] Y. Kagiyama, J.L. Hill, L.S. Gettes, Interaction of Acidosis and Increased Extracellular Potassium on Action Potential Characteristics and Conduction in Guinea Pig Ventricular Muscle, Circ. Res. 51 (1982) 614–623. https://doi.org/10.1161/01.res.51.5.614.
[17] N. Saegusa, E. Moorhouse, R.D. Vaughan-Jones, K.W. Spitzer, Influence of pH on Ca^{2+} current and its control of electrical and Ca^{2+} signaling in ventricular myocytes, J. Gen. Physiol. 138 (2011) 537–559. https://doi.org/10.1085/jgp.201110658.
[18] J. Senges, J. Brachmann, D. Pelzer, T. Mizutani, W. Kübler, Effects of some components of ischemia on electrical activity and reentry in the canine ventricular conducting system, Circ. Res. 44 (1979) 864–872. https://doi.org/10.1161/01.RES.44.6.864.
[19] B. Trénor, L. Romero, J.M. Ferrero, J. Sáiz, G. Moltó, J.M. Alonso, Vulnerability to reentry in a regionally ischemic tissue: A simulation study, Ann. Biomed. Eng. 35 (2007) 1756–1770. https://doi.org/10.1007/s10439-007-9353-3.
[20] J.M. Ferrero, B. Trénor, F. Montilla, J. Sáiz, J.M. Alonso, G. Moltó, Vulnerability to reentry during the acute phase of myocardial ischemia: A simulation study, in: Comput. Cardiol., IEEE Computer Society, 2003: pp. 425–428. https://doi.org/10.1109/cic.2003.1291183.
[21] R. Coronel, F.J.G. Wilms-Schopman, L.R.C. Dekker, M.J. Janse, Heterogeneities in $[K^+]_o$ and TQ Potential and the Inducibility of Ventricular Fibrillation During Acute Regional Ischemia in the Isolated Perfused Porcine Heart, Circulation. 92 (1995) 120–129. https://doi.org/10.1161/01.CIR.92.1.120.
[22] A.M. Tobar, J.M. Ferrero, F. Migliavacca, J.F. Rodríguez Matas, Vulnerability in regionally ischemic human heart. Effect of the extracellular potassium concentration, J. Comput. Sci. 24 (2018) 160–168. https://doi.org/10.1016/j.jocs.2017.11.009.
[23] J.M. Ferrero, V. Torres, F. Montilla, E. Colomar, Simulation of reentry during acute myocardial ischemia: role of ATP-sensitive potassium current and acidosis, in: Comput. Cardiol., IEEE, 2000: pp. 239–242. https://doi.org/10.1109/cic.2000.898501.

[24] P.B. Tabereaux, G.P. Walcott, J.M. Rogers, J. Kim, D.J. Dosdall, P.G. Robertson, C.R. Killingsworth, W.M. Smith, R.E. Ideker, Activation patterns of Purkinje fibers during long-duration ventricular fibrillation in an isolated canine heart model, Circulation. 116 (2007) 1113–1119. https://doi.org/10.1161/CIRCULATIONAHA.107.699264.
[25] M.J. Janse, F.J.G. Wilms-Schopman, R. Coronel, Ventricular Fibrillation Is Not Always Due to Multiple Wavelet Reentry, J. Cardiovasc. Electrophysiol. 6 (1995) 512–521. https://doi.org/10.1111/j.1540-8167.1995.tb00424.x.
[26] D.J. Dosdall, P.B. Tabereaux, J.J. Kim, G.P. Walcott, J.M. Rogers, C.R. Killingsworth, J. Huang, P.G. Robertson, W.M. Smith, R.E. Ideker, Chemical ablation of the Purkinje system causes early termination and activation rate slowing of long-duration ventricular fibrillation in dogs, Am J Physiol Hear. Circ Physiol. 295 (2008) H883–H889. https://doi.org/10.1152/ajpheart.00466.2008.
[27] H. Martinez-Navarro, A. Mincholé, A. Bueno-Orovio, B. Rodriguez, High arrhythmic risk in antero-septal acute myocardial ischemia is explained by increased transmural reentry occurrence, Sci. Rep. 9 (2019) 1–12. https://doi.org/10.1038/s41598-019-53221-2.
[28] M. Deo, P. Boyle, G. Plank, E. Vigmond, Arrhythmogenic mechanisms of the Purkinje system during electric shocks: A modeling study, Hear. Rhythm. 6 (2009) 1782–1789. https://doi.org/10.1016/j.hrthm.2009.08.023.
[29] M.E. Martinez, R.D. Walton, J.D. Bayer, M. Haïssaguerre, E.J. Vigmond, M. Hocini, O. Bernus, Role of the Purkinje-Muscle Junction on the Ventricular Repolarization Heterogeneity in the Healthy and Ischemic Ovine Ventricular Myocardium, Front. Physiol. 9 (2018) 718. https://doi.org/10.3389/fphys.2018.00718.
[30] T. Lassila, M. Lange, A.R. Porras Perez, K. Lekadir, X. Albà, G. Piella, A.F. Frangi, Electrophysiology Model for a Human Heart with Ischemic Scar and Realistic Purkinje Network, in: O. Camara, T. Mansi, M. Pop, K. Rhode, M. Sermesant, A. Young (Eds.), Stat. Atlases Comput. Model. Hear. Imaging Model. Challenges, Springer International Publishing, Cham, 2016: pp. 90–97.
[31] A. Lopez-Perez, R. Sebastian, M. Izquierdo, R. Ruiz, M. Bishop, J.M. Ferrero, Personalized cardiac computational models: From clinical data to simulation of infarct-related ventricular tachycardia, Front. Physiol. 10 (2019) 580. https://doi.org/10.3389/fphys.2019.00580.
[32] CIBC, Seg3D: Volumetric Image Segmentation and Visualization. Scientific Computing and Imaging Institute (SCI), (2016). http://www.seg3d.org.
[33] S. Sicouri, C. Antzelevitch, A subpopulation of cells with unique electrophysiological properties in the deep subepicardium of the canine ventricle. The M cell, Circ. Res. 68 (1991) 1729–1741. https://doi.org/10.1161/01.RES.68.6.1729.
[34] S. Sicouri, J. Fish, C. Antzelevitch, Distribution of M Cells in the Canine Ventricle, J. Cardiovasc. Electrophysiol. 5 (1994) 824–837. https://doi.org/10.1111/j.1540-8167.1994.tb01121.x.
[35] G.-X. Yan, W. Shimizu, C. Antzelevitch, Characteristics and Distribution of M Cells in Arterially Perfused Canine Left Ventricular Wedge Preparations, Circulation. 98 (1998) 1921–1927. https://doi.org/10.1161/01.CIR.98.18.1921.
[36] D.D. Streeter Jr., H.M. Spotnitz, D.P. Patel, J. Ross, E.H. Sonnenblick, Fiber Orientation in the Canine Left Ventricle during Diastole and Systole, Circ. Res. 24 (1969) 339–347. https://doi.org/10.1161/01.RES.24.3.339.
[37] J.T. Ortiz-Pérez, J. Rodríguez, S.N. Meyers, D.C. Lee, C. Davidson, E. Wu, Correspondence Between the 17-Segment Model and Coronary Arterial Anatomy Using Contrast-Enhanced Cardiac Magnetic Resonance Imaging, JACC Cardiovasc. Imaging. 1 (2008) 282–293. https://doi.org/10.1016/j.jcmg.2008.01.014.
[38] S. Dutta, A. Mincholé, E. Zacur, T.A. Quinn, P. Taggart, B. Rodriguez, Early afterdepolarizations promote transmural reentry in ischemic human ventricles with reduced repolarization reserve, Prog. Biophys. Mol. Biol. 120 (2016) 236–248. https://doi.org/10.1016/j.pbiomolbio.2016.01.008.
[39] D.A. Geerse, K.C. Wu, A.P. Gorgels, J. Zimmet, G.S. Wagner, J.M. Miller, Comparison between contrast-enhanced magnetic resonance imaging and selvester qrs scoring system in estimating changes in infarct size between the acute and chronic phases of myocardial infarction, Ann. Noninvasive Electrocardiol. 14 (2009) 360–365. https://doi.org/10.1111/J.1542-474X.2009.00327.X.
[40] W.N.W.A. Naim, M.J.M. Mokhtarudin, E. Lim, B.T. Chan, A.A. Bakir, N.A.N. Mohamed, The study of border zone formation in ischemic heart using electro-chemical coupled computational model, Int. j. Numer. Method. Biomed. Eng. 36 (2020) e3398. https://doi.org/10.1002/CNM.3398.
[41] G. Ertl, S. Frantz, Healing after myocardial infarction, Cardiovasc. Res. 66 (2005) 22–32. https://doi.org/10.1016/J.CARDIORES.2005.01.011.

[42] R.J. Kim, D.S. Fieno, T.B. Parrish, K. Harris, E.-L. Chen, O. Simonetti, J. Bundy, J.P. Finn, F.J. Klocke, R.M. Judd, Relationship of MRI Delayed Contrast Enhancement to Irreversible Injury, Infarct Age, and Contractile Function, Circulation. 100 (1999) 1992–2002. https://doi.org/10.1161/01.CIR.100.19.1992.
[43] E.F. Carpio, J.F. Gomez, R. Sebastian, A. Lopez-Perez, E. Castellanos, J. Almendral, J.M. Ferrero, B. Trenor, Optimization of lead placement in the right ventricle during cardiac resynchronization therapy. A simulation study, Front. Physiol. 10 (2019) 74. https://doi.org/10.3389/fphys.2019.00074.
[44] R. Sebastian, V. Zimmerman, D. Romero, D. Sanchez-Quintana, A.F. Frangi, Characterization and modeling of the peripheral cardiac conduction system, IEEE Trans. Med. Imaging. 32 (2013) 45–55. https://doi.org/10.1109/TMI.2012.2221474.
[45] C. Mendez, W.J. Mueller, X. Urguiaga, Propagation of Impulses across the Purkinje Fiber-Muscle Junctions in the Dog Heart, Circ. Res. 26 (1970) 135–150. https://doi.org/10.1161/01.RES.26.2.135.
[46] A. Ferrer, R. Sebastián, D. Sánchez-Quintana, J.F. Rodríguez, E.J. Godoy, L. Martínez, J. Saiz, Detailed Anatomical and Electrophysiological Models of Human Atria and Torso for the Simulation of Atrial Activation, PLoS One. 10 (2015) e0141573. https://doi.org/10.1371/journal.pone.0141573.
[47] T. O'Hara, L. Virág, A. Varró, Y. Rudy, Simulation of the Undiseased Human Cardiac Ventricular Action Potential: Model Formulation and Experimental Validation, PLOS Comput. Biol. 7 (2011) e1002061. https://doi.org/10.1371/journal.pcbi.1002061.
[48] M. Gironés-Sangüesa, C. Esteban, A. González-Ascaso, J.F. Rodríguez-Matas, J.F. Ferrero, A Novel Model of Acute Myocardial Ischemia in Human Ventricular Cardiomyocytes, in: 2020 Comput. Cardiol., 2020: pp. 1–4. https://doi.org/10.22489/CinC.2020.405.
[49] E.F. Carpio, J.F. Gomez, J.F. Rodríguez-Matas, B. Trenor, J.M. Ferrero, Computational analysis of vulnerability to reentry in acute myocardial ischemia, in: 2020 Comput. Cardiol., 2020: pp. 1–4. https://doi.org/10.22489/CinC.2020.241.
[50] A.P. Babenko, G. Gonzalez, L. Aguilar-Bryan, J. Bryan, Reconstituted Human Cardiac K_{ATP} Channels, Circ. Res. 83 (1998) 1132–1143. https://doi.org/10.1161/01.RES.83.11.1132.
[51] S. Cortassa, M.A. Aon, B. O'Rourke, R. Jacques, H.J. Tseng, E. Marbán, R.L. Winslow, A computational model integrating electrophysiology, contraction, and mitochondrial bioenergetics in the ventricular myocyte, Biophys. J. 91 (2006) 1564–1589. https://doi.org/10.1529/biophysj.105.076174.
[52] L. Murphy, D. Renodin, C. Antzelevitch, J.M. Di Diego, J.M. Cordeiro, Extracellular proton depression of peak and late Na^+ current in the canine left ventricle, Am. J. Physiol. Circ. Physiol. 301 (2011) H936–H944. https://doi.org/10.1152/ajpheart.00204.2011.
[53] C.L. Watson, M.R. Gold, Effect of intracellular and extracellular acidosis on sodium current in ventricular myocytes, Am. J. Physiol. 268 (1995) H1749–H1756. https://doi.org/10.1152/ajpheart.1995.268.4.H1749.
[54] A.E. Doering, D.A. Eisner, W.J. Lederer, Cardiac Na-Ca Exchange and pH, Ann. N. Y. Acad. Sci. 779 (1996) 182–198. https://doi.org/10.1111/j.1749-6632.1996.tb44786.x.
[55] M. Egger, E. Niggli, Paradoxical block of the Na^+-Ca^{2+} exchanger by extracellular protons in guinea-pig ventricular myocytes, J. Physiol. 523 (2000) 353–366. https://doi.org/10.1111/j.1469-7793.2000.t01-1-00353.x.
[56] P. Daleau, Lysophosphatidylcholine, a metabolite which accumulates early in myocardium during ischemia, reduces gap junctional coupling in cardiac cells, J. Mol. Cell. Cardiol. 31 (1999) 1391–1401. https://doi.org/10.1006/jmcc.1999.0973.
[57] M. Gautier, H. Zhang, I.M. Fearon, Peroxynitrite formation mediates LPC-induced augmentation of cardiac late sodium currents, J. Mol. Cell. Cardiol. 44 (2008) 241–251. https://doi.org/10.1016/j.yjmcc.2007.09.007.
[58] A.I. Undrovinas, I.A. Fleidervish, J.C. Makielski, Inward sodium current at resting potentials in single cardiac myocytes induced by the ischemic metabolite lysophosphatidylcholine, Circ. Res. 71 (1992) 1231–1241. https://doi.org/10.1161/01.RES.71.5.1231.
[59] K. Sakamoto, M. Ishikawa, K. Koga, T. Urushidani, T. Nagao, Energy Preserving Effect of l-cis Diltiazem in Isolated Ischemic and Reperfused Guinea Pig Hearts. A 31P-NMR Study, Jpn. J. Pharmacol. 83 (2000) 225–232. https://doi.org/10.1254/jjp.83.225.
[60] W.F. Fleet, T.A. Johnson, C.A. Graebner, L.S. Gettes, Effect of serial brief ischemic episodes on extracellular K+, pH, and activation in the pig, Circulation. 72 (1985) 922–932. https://doi.org/10.1161/01.CIR.72.4.922.
[61] J. Weiss, K.I. Shine, Extracellular potassium accumulation during myocardial ischemia: Implications

for arrhythmogenesis, J. Mol. Cell. Cardiol. 13 (1981) 699–704. https://doi.org/10.1016/0022-2828(81)90277-7.
[62] J.L. Hill, L.S. Gettes, Effect of acute coronary artery occlusion on local myocardial extracellular K^+ activity in swine, Circulation. 61 (1980) 768–778. https://doi.org/10.1161/01.CIR.61.4.768.
[63] H. Hirche, C. Franz, L. Bös, R. Bissig, R. Lang, M. Schramm, Myocardial extracellular K^+ and H^+ increase and noradrenaline release as possible cause of early arrhythmias following acute coronary artery occlusion in pigs, J. Mol. Cell. Cardiol. 12 (1980) 579–593. https://doi.org/10.1016/0022-2828(80)90016-4.
[64] V. Wiegand, M. Güggi, W. Meesmann, M. Kessler, F. Greitschus, Extracellular potassium activity changes in the canine myocardium after acute coronary occlusion and the influence of beta-blockade, Cardiovasc. Res. 13 (1979) 297–302. https://doi.org/10.1093/cvr/13.5.297.
[65] R. Coronel, J.W. Fiolet, F.J. Wilms-Schopman, A.F. Schaapherder, T.A. Johnson, L.S. Gettes, M.J. Janse, Distribution of extracellular potassium and its relation to electrophysiologic changes during acute myocardial ischemia in the isolated perfused porcine heart, Circulation. 77 (1988) 1125–1138. https://doi.org/10.1161/01.CIR.77.5.1125.
[66] R.L. Wilensky, J. Tranum-Jensen, R. Coronel, A.A. Wilde, J.W. Fiolet, M.J. Janse, The subendocardial border zone during acute ischemia of the rabbit heart: an electrophysiologic, metabolic, and morphologic correlative study, Circulation. 74 (1986) 1137–1146. https://doi.org/10.1161/01.CIR.74.5.1137.
[67] P. Stewart, O. V. Aslanidi, D. Noble, P.J. Noble, M.R. Boyett, H. Zhang, Mathematical models of the electrical action potential of Purkinje fibre cells, Philos. Trans. R. Soc. A Math. Phys. Eng. Sci. 367 (2009) 2225–2255. https://doi.org/10.1098/rsta.2008.0283.
[68] M.J. Janse, F.J. van Capelle, H. Morsink, A.G. Kléber, F. Wilms-Schopman, R. Cardinal, C.N. d'Alnoncourt, D. Durrer, Flow of "injury" current and patterns of excitation during early ventricular arrhythmias in acute regional myocardial ischemia in isolated porcine and canine hearts. Evidence for two different arrhythmogenic mechanisms, Circ. Res. 47 (1980) 151–165. https://doi.org/10.1161/01.RES.47.2.151.
[69] E.A. Heidenreich, J.M. Ferrero, M. Doblaré, J.F. Rodríguez, Adaptive macro finite elements for the numerical solution of monodomain equations in cardiac electrophysiology, Ann. Biomed. Eng. 38 (2010) 2331–2345. https://doi.org/10.1007/s10439-010-9997-2.
[70] P. Taggart, P.M. Sutton, T. Opthof, R. Coronel, R. Trimlett, W. Pugsley, P. Kallis, Inhomogeneous transmural conduction during early ischaemia in patients with coronary artery disease, J. Mol. Cell. Cardiol. 32 (2000) 621–630. https://doi.org/10.1006/jmcc.2000.1105.
[71] D. Durrer, R.T. Van Dam, G.E. Freud, M.J. Janse, F.L. Meijler, R.C. Arzbaecher, Total Excitation of the Isolated Human Heart, Circulation. 41 (1970) 899–912. https://doi.org/10.1161/01.CIR.41.6.899.
[72] L. Dux-Santoy, R. Sebastian, J.F. Rodriguez, J.M. Ferrero, Modeling the different sections of the cardiac conduction system to obtain realistic electrocardiograms, in: Proc. Annu. Int. Conf. IEEE Eng. Med. Biol. Soc. EMBS, 2013: pp. 6846–6849. https://doi.org/10.1109/EMBC.2013.6611130.
[73] M. Potse, B. Dube, J. Richer, A. Vinet, R.M. Gulrajani, A Comparison of Monodomain and Bidomain Reaction-Diffusion Models for Action Potential Propagation in the Human Heart, IEEE Trans. Biomed. Eng. 53 (2006) 2425–2435. https://doi.org/10.1109/TBME.2006.880875.
[74] D.U.J. Keller, F.M. Weber, G. Seemann, O. Dössel, Ranking the Influence of Tissue Conductivities on Forward-Calculated ECGs, IEEE Trans. Biomed. Eng. 57 (2010) 1568–1576. https://doi.org/10.1109/TBME.2010.2046485.
[75] B.J. Boukens, M.R. Rivaud, S. Rentschler, R. Coronel, Misinterpretation of the mouse ECG: "Musing the waves of Mus musculus," J. Physiol. 592 (2014) 4613–4626. https://doi.org/10.1113/jphysiol.2014.279380.
[76] A.L. Goldberger, L.A. Amaral, L. Glass, J.M. Hausdorff, P.C. Ivanov, R.G. Mark, J.E. Mietus, G.B. Moody, C.K. Peng, H.E. Stanley, PhysioBank, PhysioToolkit, and PhysioNet: components of a new research resource for complex physiologic signals, Circulation. 101 (2000). https://doi.org/10.1161/01.cir.101.23.e215.
[77] J. Pettersson, E. Carro, L. Edenbrandt, C. Maynard, O. Pahlm, M. Ringborn, L. Sörnmo, S.G. Warren, G.S. Wagner, Spatial, individual, and temporal variation of the high-frequency QRS amplitudes in the 12 standard electrocardiographic leads, Am. Heart J. 139 (2000) 352–358. https://doi.org/10.1016/S0002-8703(00)90246-1.
[78] S. Mahendrappa, T. Sathyanarayana, The normal variations in heart rate and QRS complex of healthy individuals in different age groups, Int. J. Res. Med. Sci. 2 (2014) 861–865.

https://doi.org/10.5455/2320-6012.ijrms20140821.
[79] J. Wu, J.A. Kors, P.R. Rijnbeek, G. Van Herpen, Z. Lu, C. Xu, Normal limits of the electrocardiogram in Chinese subjects, Int. J. Cardiol. 87 (2003) 37–51. https://doi.org/10.1016/S0167-5273(02)00248-6.
[80] K. Channer, F. Morris, ABC of clinical electrocardiography: Myocardial ischaemia, BMJ. 324 (2002) 1023–1026. https://doi.org/10.1136/bmj.324.7344.1023.
[81] E.B. Hanna, D.L. Glancy, ST-segment depression and T-wave inversion: Classification, differential diagnosis, and caveats, Cleve. Clin. J. Med. 78 (2011) 404–414. https://doi.org/10.3949/ccjm.78a.10077.
[82] E.B. Sgarbossa, S.L. Pinski, A. Barbagelata, D.A. Underwood, K.B. Gates, E.J. Topol, R.M. Califf, G.S. Wagner, Electrocardiographic Diagnosis of Evolving Acute Myocardial Infarction in the Presence of Left Bundle-Branch Block, N. Engl. J. Med. 334 (1996) 481–487. https://doi.org/10.1056/NEJM199602223340801.
[83] S.W. Smith, K.W. Dodd, T.D. Henry, D.M. Dvorak, L.A. Pearce, Diagnosis of ST-elevation myocardial infarction in the presence of left bundle branch block with the ST-elevation to S-wave ratio in a modified sgarbossa rule, Ann. Emerg. Med. 60 (2012) 766–776. https://doi.org/10.1016/j.annemergmed.2012.07.119.
[84] P.M.I. Sutton, P. Taggart, T. Opthof, R. Coronel, R. Trimlett, W. Pugsley, P. Kallis, Repolarisation and refractoriness during early ischaemia in humans, Heart. 84 (2000) 365–369. https://doi.org/10.1136/heart.84.4.365.
[85] R.D. Walton, M.E. Martinez, M.J. Bishop, M. Lè Ze Hocini, M.H. Haı̈ssaguerre, G. Plank, O. Bernus, E.J. Vigmond, Influence of the Purkinje-muscle junction on transmural repolarization heterogeneity, Cardiovasc. Res. 103 (2014) 629–640. https://doi.org/10.1093/cvr/cvu165.
[86] R.D. Walton, A.P. Benson, M.E.L. Hardy, E. White, O. Bernus, Electrophysiological and structural determinants of electrotonic modulation of repolarization by the activation sequence, Front. Physiol. 4 (2013) 281. https://doi.org/10.3389/fphys.2013.00281.
[87] F.L. Burton, S.M. Cobbe, Dispersion of ventricular repolarization and refractory period, Cardiovasc. Res. 50 (2001) 10–23. https://doi.org/10.1016/S0008-6363(01)00197-3.
[88] A.G. Kléber, M.J. Janse, F.J. van Capelle, D. Durrer, Mechanism and time course of S-T and T-Q segment changes during acute regional myocardial ischemia in the pig heart determined by extracellular and intracellular recordings, Circ. Res. 42 (1978) 603–613. https://doi.org/10.1161/01.RES.42.5.603.
[89] S. Dutta, A. Mincholé, T.A. Quinn, B. Rodriguez, Electrophysiological properties of computational human ventricular cell action potential models under acute ischemic conditions, Prog. Biophys. Mol. Biol. 129 (2017) 40–52. https://doi.org/10.1016/j.pbiomolbio.2017.02.007.
[90] C. Costeas, N.S. Peters, B. Waldecker, E.J. Ciaccio, A.L. Wit, J. Coromilas, Mechanisms Causing Sustained Ventricular Tachycardia With Multiple QRS Morphologies, Circulation. 96 (1997) 3721–3731. https://doi.org/10.1161/01.CIR.96.10.3721.
[91] M.J. Janse, J. Cinca, H. Moréna, J.W. Fiolet, A.G. Kléber, G.P. de Vries, A.E. Becker, D. Durrer, The "border zone" in myocardial ischemia. An electrophysiological, metabolic, and histochemical correlation in the pig heart, Circ. Res. 44 (1979) 576–588. https://doi.org/10.1161/01.RES.44.4.576.
[92] E. Kaplinsky, S. Ogawa, C.W. Balke, L.S. Dreifus, Two periods of early ventricular arrhythmia in the canine acute myocardial infarction model, Circulation. 60 (1979) 397–403. https://doi.org/10.1161/01.CIR.60.2.397.
[93] A.G. Kléber, Extracellular potassium accumulation in acute myocardial ischemia, J. Mol. Cell. Cardiol. 16 (1984) 389–394. https://doi.org/10.1016/S0022-2828(84)80610-0.
[94] C.H. Luo, Y. Rudy, A dynamic model of the cardiac ventricular action potential. I. Simulations of ionic currents and concentration changes, Circ. Res. 74 (1994) 1071–1096. https://doi.org/10.1161/01.RES.74.6.1071.
[95] K.H.W.J. Ten Tusscher, D. Noble, P.J. Noble, A. V. Panfilov, A model for human ventricular tissue, Am. J. Physiol. - Hear. Circ. Physiol. 286 (2004) 1573–1589. https://doi.org/10.1152/ajpheart.00794.2003.
[96] B.A.J. Lawson, R.S. Oliveira, L.A. Berg, P.A.A. Silva, K. Burrage, R.W. dos Santos, Variability in electrophysiological properties and conducting obstacles controls re-entry risk in heterogeneous ischaemic tissue, Philos. Trans. R. Soc. A Math. Phys. Eng. Sci. 378 (2020) 20190341. https://doi.org/10.1098/rsta.2019.0341.
[97] A.A.M. Wilde, Role of ATP-sensitive K^+ channel current in ischemic arrhythmias, Cardiovasc. Drugs

Ther. 7 (1993) 521–526. https://doi.org/10.1007/BF00877617.
[98] M. Said, R. Becerra, J. Palomeque, G. Rinaldi, M.A. Kaetzel, P.L. Diaz-Sylvester, J.A. Copello, J.R. Dedman, C. Mundiña-Weilenmann, L. Vittone, A. Mattiazzi, Increased intracellular Ca^{2+} and SR Ca^{2+} load contribute to arrhythmias after acidosis in rat heart. Role of Ca^{2+}/calmodulin-dependent protein kinase II, Am. J. Physiol. Circ. Physiol. 295 (2008) H1669–H1683. https://doi.org/10.1152/ajpheart.00010.2008.
[99] Y.M. Cha, T. Uchida, P.L. Wolf, B.B. Peters, M.C. Fishbein, H.S. Karagueuzian, P.S. Chen, Effects of chemical subendocardial ablation on activation rate gradient during ventricular fibrillation, Am. J. Physiol. - Hear. Circ. Physiol. 269 (1995) H1998–H2009. https://doi.org/10.1152/ajpheart.1995.269.6.h1998.
[100] C. Livia, A. Sugrue, T. Witt, M.D. Polkinghorne, E. Maor, S. Kapa, H.I. Lehmann, C. V. DeSimone, A. Behfar, S.J. Asirvatham, C.J. McLeod, Elimination of Purkinje Fibers by Electroporation Reduces Ventricular Fibrillation Vulnerability, J. Am. Heart Assoc. 7 (2018) e009070. https://doi.org/10.1161/JAHA.118.009070.
[101] M.J. Janse, A.G. Kleber, A. Capucci, R. Coronel, F. Wilms-Schopman, Electrophysiological basis for arrhythmias caused by acute ischemia. Role of the subendocardium, J. Mol. Cell. Cardiol. 18 (1986) 339–355. https://doi.org/10.1016/S0022-2828(86)80898-7.
[102] E. Behradfar, A. Nygren, E.J. Vigmond, The Role of Purkinje-Myocardial Coupling during Ventricular Arrhythmia: A Modeling Study, PLoS One. 9 (2014) e88000. https://doi.org/10.1371/journal.pone.0088000.
[103] P.L. Friedman, J.R. Stewart, J.J. Fenoglio, A.L. Wit, Survival of Subendocardial Purkinje Fibers after Extensive Myocardial Infarction in Dogs, Circ. Res. 33 (1973) 597–611. https://doi.org/10.1161/01.RES.33.5.597.
[104] P.F. Cranefield, H.O. Klein, B.F. Hoffman, Conduction of the cardiac impulse. 1. Delay, block, and one-way block in depressed Purkinje fibers, Circ. Res. 28 (1971) 199–219. https://doi.org/10.1161/01.RES.28.2.199.
[105] A.L. Wit, B.F. Hoffman, P.F. Cranefield, Slow Conduction and Reentry in the Ventricular Conducting System. I. Return extrasystole in canine Purkinje fibers, Circ. Res. 30 (1972) 1–10. https://doi.org/10.1161/01.RES.30.1.1.
[106] W.J. Penny, D.J. Sheridan, Arrhythmias and cellular electrophysiological changes during myocardial "ischaemia" and reperfusion, Cardiovasc. Res. 17 (1983) 363–372. https://doi.org/10.1093/cvr/17.6.363.
[107] K.D. Chadda, V.S. Banka, R.H. Helfant, Rate Dependent Ventricular Ectopia Following Acute Coronary Occlusion, Circulation. 49 (1974) 654–658. https://doi.org/10.1161/01.CIR.49.4.654.
[108] R.J. Sung, W.A. Shapiro, E.N. Shen, F. Morady, J. Davis, Effects of verapamil on ventricular tachycardias possibly caused by reentry, automaticity, and triggered activity, J. Clin. Invest. 72 (1983) 350–360. https://doi.org/10.1172/JCI110975.
[109] K.I. Lie, J.J. Wellens, E. Downar, D. Durrer, Observations on Patients with Primary Ventricular Fibrillation Complicating Acute Myocardial Infarction, Circulation. 52 (1975) 755–759. https://doi.org/10.1161/01.cir.52.5.755.
[110] R.F. Gilmour, D.P. Zipes, Different electrophysiological responses of canine endocardium and epicardium to combined hyperkalemia, hypoxia, and acidosis, Circ. Res. 46 (1980) 814–825. https://doi.org/10.1161/01.RES.46.6.814.
[111] R. Lazzara, N. El-Sherif, B.J. Scherlag, Early and Late Effects of Coronary Artery Occlusion on Canine Purkinje Fibers, Circ. Res. 35 (1974) 391–399. https://doi.org/10.1161/01.RES.35.3.391.

Supporting information

Video 1. Reentrant pattern of a macro-reentry using the biventricular/torso model. (Left) Action potentials recorded in different locations of the myocardium. (Middle) Ventricular potential maps that show the generation of a figure-of-eight reentry. (Right) Body surface potential maps and ECG recorded at precordial leads during the reentry. The simulated ischemic conditions were moderate hyperkalemia and acidosis, and severe anoxia. Coupling interval: 320 ms.

Video 2. Effect of His-Purkinje system on reentry. (Top row) Macro-reentry obtained in the model with His-Purkinje system during moderate ischemia. (Bottom row) No reentry in the simulation under the same ischemic conditions using the model without His-Purkinje system. Reentrant activity started with a premature stimulus (S2) in the right border zone occurring 340 ms after the fifth sinus beat.